DEVELOPMENT OF TESTS TO SIMULATE USE CONDITIONS AND FABRICATION OF ADDITIVELY MANUFACTURED CERAMIC NOZZLES

BY

TIMOTHY R. MAHANY

A THESIS
SUBMITTED TO THE FACULTY OF

ALFRED UNIVERSITY

IN PARTIAL FULFILLMENT OF THE REQUIREMENTS
FOR THE DEGREE OF

MASTER OF SCIENCE

IN

MATERIALS SCIENCE AND ENGINEERING

ALFRED, NEW YORK

April, 2022

DEVELOPMENT OF TESTS TO SIMULATE USE CONDITIONS AND FABRICATION OF ADDITIVELY MANUFACTURED CERAMIC NOZZLES

BY

TIMOTHY R. MAHANY

B.S. ALFRED UNIVERSITY (2020)

SIGNATURE OF AUTHOR_____

APPROVED BY_____

Dr. HOLLY SHULMAN, ADVISOR

_____

Dr. S. K. SUNDARAM, ADVISORY COMMITTEE

_____

Dr. JUNJUN DING, ADVISORY COMMITTEE

_____

Dr. DORIS MÖNCKE, CHAIR, ORAL THESIS DEFENSE

ACCEPTED BY_____

Dr. GABRIELLE G. GAUSTAD, DEAN
KAZUO INAMORI SCHOOL OF ENGINEERING

ACKNOWLEDGMENTS

I want to thank Dr. Holly Shulman, my graduate thesis advisor, for her support and guidance over the course my graduate career in addition for her advice throughout my undergraduate career. She helped to expand knowledge and learn new topics which are all beneficial towards advancing my professional career. I also want to thank Dr. Junjun Ding and Dr. S.K. Sundaram, my thesis committee, for their time, assistance, and continued support throughout my graduate studies.

I expressed gratitude towards all the staff at Alfred University. Especially, Dr. Darren Stohr who was willing to answer my questions and provide support no matter how often I came knocking. Francis Williams for his assistance with various technical instruments.

Ryan Fordham, Kade McGarrity, Dan Delia, and Nick Tostanoski were fellow graduate students who throughout my studies were a valuable resource who assisted by providing advice or guidance on how to overcome challenges. They were always ready to lend a hand (or ear) and give suggestions or recommendations on how to overcome roadblocks that would arise.

Len Zima, Jason Jones, Barry Safier, and the group at MOOG Inc. for their knowledge and time throughout the project. This project would not have happened if it was not for their dedication to purse this collaboration, and for MOOG Inc. which provided finical support for this project.

Shawn Allan and the amazing group of individuals over at Lithoz America LLC for their technical assistance and advice on overcoming challenges. Their excitement and willingness to help was extremely beneficial and appreciated.

Lastly, I am very thankful for my family Bob, Kathi, Bobby, and Danny who have always supported me throughout my continued education. All of them have pushed me to keep going.

TABLE OF CONTENTS

Page

LIST OF TABLES

Page

LIST OF FIGURES

Page

ABSTRACT

Additive manufacturing (AM) allows for the rapid production of a desired shape, and enables the ability to modify the design before it is produced again. This can be a valuable tool in industry as a method for manufacturing prototypes, and larger runs of the same part, to an extent. There is a cost/benefit tipping point that is influenced by the complexity of the part, number of parts needed, frequency and value of design modifications, quality of parts produced, turnaround time, skill level of labor, infrastructure, profit margin for product, and other factors. AM of ceramics has lagged behind polymers and metals, as ceramic fabrication includes issues of shrinkage, distortion, and strength limiting process flaws. This AM alumina work was stimulated by a need in aerospace applications for a ceramic nozzle to replace a machined high temperature precious metal. This nozzle is an excellent test case for the rapid response of AM to develop a high value ceramic part.

Technical ceramics can have superior characteristics, such as the ability to withstand high temperatures and high compressive forces, compared to other materials. Lithography-based Ceramic Manufacturing (LCM) is one of the current techniques that can be used for AM of ceramics. This work focused on producing nozzles out of Al_2O_3 by means of LCM, and then subjecting the printed parts to internal pressure and thermal shock tests. To conduct pressure tests on the samples a custom apparatus had to be designed and produced to hold the sample while allowing the freedom to select the pressure that was applied. The testing jig was electronically controlled and allowed for a max pressure of 6.9 MPa (1,000 psi) to be tested. The printed Al_2O_3 parts were thermally shocked once to four different ΔT's; 300° C, 500° C, 700° C, 900° C. Each ΔT were then rapidly internally pressurized up to 205 times to two different pressures; 3.4 MPa (500 psi), 6.9 MPa (1,000 psi). The ΔT's of 300°C and 500°C showed they could survive being thermally shocked and survive 6.9 MPa (1,000 psi). Whereas samples that had a ΔT of 700° C and 900° C received critical damage from being thermally shocked and could not handle any pressure.

I. INTRODUCTION

Technical ceramics have advantages over polymers and metals, e.g. the ability to withstand high temperatures, insulating characteristics, wear and corrosion resistance, and the ability to withstand high compressive forces. Their over-all compressive strength and hardness drops slightly at elevated temperatures[1]. High performance ceramics have superior properties when it comes to handling high temperatures as some can withstand temperatures above 2,000° C (3,632° F)[2].

A common traditional manufacturing process for ceramics is injection molding. This method can be used for mass production of a single geometry, however this process has a high upfront cost and the use of an expensive mold makes it impossible to easily modify the part design. Injection molding has limited design freedom as certain features and geometries simply cannot be made through this process. In injection modeling the part needs to be able to be remove from the mold after it was cast, restricting the overall design of the part. Machining of ceramics, once the material has been fully sintered, is difficult due to the lack of facture toughness of ceramics. It is possible, but to do so is a timely and expensive process due to the specialty tooling and equipment that is required. Ideally, near-net-shape forming of ceramics with minimal post processing would decrease small-batch production time and cost.

Additive manufacturing (AM) works to bring that concept, small-batch production, to reality as there is no mold needed to produce a geometry. Instead, the part is created using a computer aided design (CAD) file. This allows for a geometry to be produced quickly and the freedom to modify the design before continued production. AM is a beneficial tool for producing prototypes or low quantities of a desired part. While AM has some appealing traits, two disadvantages are 1) increased shrinkage during thermal processing and 2) a more complex thermal processing schedule, dependent on the AM technique being used.

An application was identified which requires a complex geometry and has significant benefits for rapid design changes. This part is a nozzle that will be used in propulsion systems which are still under development. AM will enable the substitution of

expensive machined refractory metals for ceramics. This work explores, fabrication and testing methods for a ceramic nozzle used in extreme propulsion conditions.

A. Background on Additive Manufacturing

AM is the process of manufacturing a three-dimensional part by depositing material, usually layer by layer, until the desired part is completed. This is ideal for producing complex geometries that would be improbable or impossible to produce using traditional manufacturing techniques, e.g. injection molding. AM of polymers and metals has been used widely for several decades but AM of ceramics has lagged behind due to challenges caused by ceramic densification and shrinkage.

There are several different techniques that can be used for AM of ceramics including powder bed fusion, material jetting, material extrusion, binder jetting, and photopolymerization. Table 1 shows some common companies that produce ceramic AM printers and which process they are using. Each process has advantages and disadvantages. Some of the techniques, e.g. photopolymerization, can produce high resolution parts while others are not able to, e.g. material extrusion[3]. Some techniques are relatively inexpensive, e.g. material extrusion, while other techniques have a high cost[3]. Certain techniques can make dense parts with high flexural strength, e.g. digital light processing, similar to values that are reached with traditional means of producing ceramic, while others e.g. powder bed fusion, are unable to reach high strengths[3].

With ceramic vat polymerization, e.g. 3DCeram and Lithoz, a binder is mixed with the ceramic powder in order to print with the material. The part then needs to be carefully thermally processed to remove the binder without compromising the integrity of the part. Whereas with material extrusion, e.g. robocasting, the rheology of the slurry is critical to producing a part. The material needs to be able to flow through a nozzle, and not collapse from the weight of itself or from the weight of the layer applied on top of it.

Table 1. Companies Producing AM Ceramic Printers Corresponding To Which Process Each Company Utilizes Based On ASTM AM Categories[4]

Category	Processes	Companies
Vat Photopolymerization	• Stereolithography • Digital Light Processing • Photopolymerization	• Lithoz GmbH (Austria) • 3DCeram (France) • Prodways (France) • Admatec (Netherlands) • DDM (USA) • Formlabs (USA)
Binder Jetting	• Multi Jet Fusion Technology	• ExOne (USA) • Voxelijet (Germany) • Tethon 3D (USA) • HP (USA)
Material Extrusion	• Robocasting • Fused Deposition/Layer Modeling • Direct Ink Writing	• Robocasting Enterprises (USA) • WASP (Italy) • nScrypt (USA)
Material Jetting	• Nano Particle Ink-Jetting • Aerosol Jet Printing	• Xjet (Israel) • OPTOMEC (USA)
Powder Bed Fusion	• Selective Laser Sintering/Melting • Electron Beam Melting • Laser Slip Casting	• *Academic*
Sheet Lamination	• Laminated Object Manufacturing	• CoorsTek • *Academic*

AM allows for more design freedom, as a wider array of geometries can be produced, compared to using traditional methods which can induce limitations on the desired geometry when designing parts. A common belief is that AM provides the ability to produce any geometry, it does not. While more unique geometries can be produced there are limitations put in place by the following factors: process, material, and machine parameter restrictions. Depending on the required geometry, some parts are more prone to fail during the printing process. In addition, parts can fail while undergoing the post processing thermal treatment[5]. Lithography-based Ceramic Manufacturing (LCM) are unable to print right angles, and the radii of curvatures, which can be produced, is limited as some radii result in cracking during the post processing thermal treatment[6].

B. Background on Lithography-based Ceramic Manufacturing (LCM)

1. Printing Process

Digital Light Processing (DLP) is a 3D printing process that uses a digital projector to flash a single image of the layer across the entire build platform at once. DLP can achieve

a faster print time for parts that utilize space in the x-axis and y-axis. When the LED projector flashes the image to cure the slurry, it takes the same amount of time regardless of how much space across the build platform (x-axis and y-axis) is being used. By using this type of light source, that is able to cover the entire cross section of the part to cure it at once, results in the part being able to be produce at a faster speed than other methods[7]. Build time increases once the part uses space in the z-axis. Lithography-based ceramic manufacturing (LCM), developed and commercialized by Lithoz[8], builds off of Digital Light Processing (DLP) which uses a light engine. Figure 1 is a diagram which shows the basic components of the system.

The light engine is based on light-emitting diodes (LEDs) and a digital micromirror device (DMD). The individual DMD chip can be tilted causing the pixels to be turned on and off individually according to the contour of the cross section that is to be projected. The system also using dedicated projection optics which helps to spread the light intensity uniformly across the build platform, from the center to the corners of the platform. The light intensity at the corners of the build platform has been measured to be 98.4% of the intensity at the center[8].

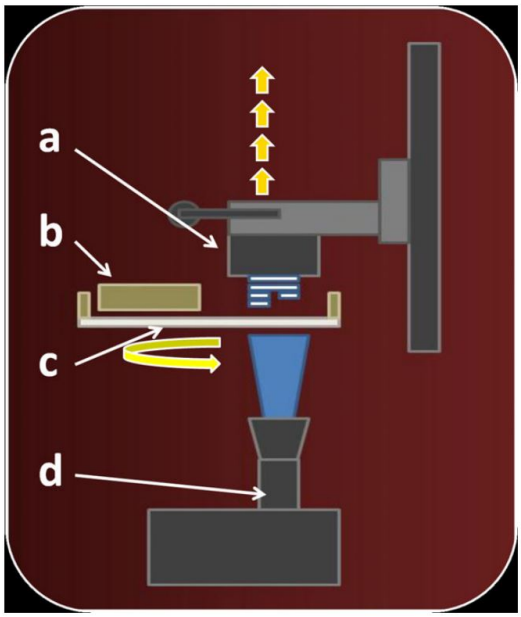

Figure 1. Schematic drawing of the LCM process which is based on Digital Light Processing: a) build platform, b) wiper blade, c) vat, d) light engine[8]

For ceramic AM there are two classifications; direct and indirect processes. DLP, and therefore LCM, is an indirect AM technique as following the printing process the part is a green body and needs to be thermal processed[3, 9]. These techniques typically are capable of producing parts that are high density, high surface quality, and have high strength valves[10]. During the printing process in order to shape the ceramic powder into the desired geometry, it is combined with a organic binder. Resulting in a green body part, ceramic particles and organic binder, upon completion of the print[11]. This means that after the part is produced it need to undergo a thermal treatment to eliminate the organic components. The thermal treatment in composed of two steps; the first is a debinding process to remove the organic binder and a subsequent sintering process to give the ceramic bodies[12].

Lithoz printers use highly viscous photopolymerizable slurries which can result in the formation of air bubbles in the material. When the build platform contacts the slurry in the vat there is a probability that air bubbles will be formed. In the Lithoz printers, one side of the platform that holds the vat is hinged to allow it to pivot while the opposite side is able to move up and down. When the build platforms descends to contact the vat the one side of the floor platform, that holds the vat, lowers. Once the build platform reaches the desired position in the z-axis, the floor platform moves back into position to be parallel to the build platform. As the floor platform moves upward to contact the slurry, it does so in a linear movement to minimize the formation of gas bubbles in the slurry[13]. The movement of the floor platform, and therefore the vat, works to push out the air bubbles out.

Inside the print envelope, the build platform is mounted upside down on a rail that moves vertically, in the y-axis, to contact the build platform with the vat. The lifting mechanism is precisely adjusting the vertical position to achieve the desired layer thickness between the build platform and the vat. Once the build platform reaches the position, the photopolymer-merizable material is exposed by position-selective exposure from below through the translucent bottom[13]. Directly below the build platform is a circular vat that holds slurry. In DLP the light engine flashes a blue light across the build platform that cures the photopolymer in the slurry. The slurry is cured when the when exposed to a light of a certain wavelength. This causes the monomers to be photopolymerized in the ceramic-filled slurry resulting in a 3-dimenstional network that forms a enclosure around

the ceramic filler[12]. Figure 2 shows an illustration of how the monomers move to form a grid pattern upon being cured by the light.

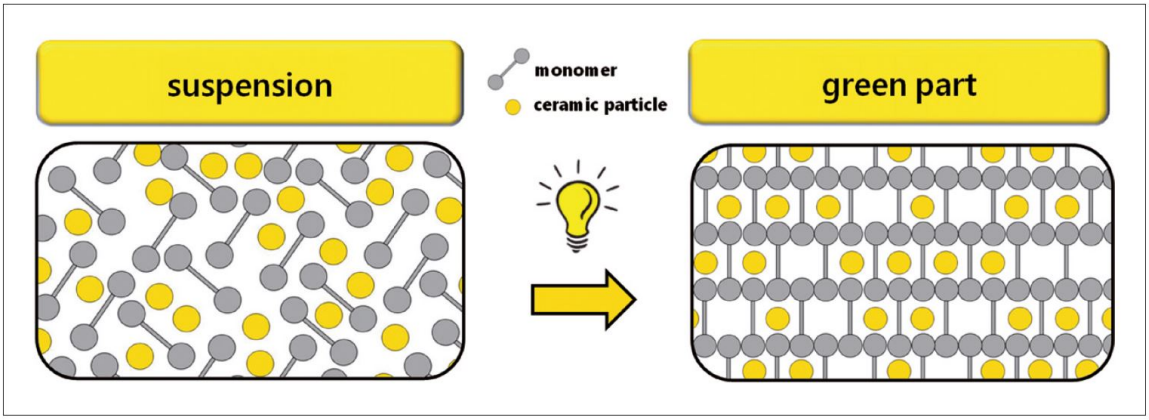

Figure 2. Illustration of the curing that happens to the ceramic suspension during the LCM printing process[12]

The vat is removable from the machine to allow for cleaning and to replace the top piece of glass if it becomes damaged during printing. Depending on the material that is being used there is a specific glass that should be used to ensure quality printing. In order to coat the vat with the correct thickness throughout the printing process a wiper blade mechanism is used. The crucial parameters for the shaping process include the thickness of the layers and the intensity of the light engine as well as the exposure time per layer[8].

When the vat is installed in the print envelope, the vat can rotate in a circular motion. There is a wiper blade that is above the vat. The wiper blade moves over the vat and tilts downward to coat the vat with slurry. The angle of the wiper blade is adjustable so the angle can be modified to apply the desired thickness of slurry to the vat. Slurry thickness is selected and set prior to starting the print. At the beginning of each individual layer the vat rotates, the number of rotations is selected prior to starting the print, and the wiper blade moves into position over the vat. It then angles downwards to push slurry in order to apply a new layer across the vat.

When setting up a print, an adhesion film needs to be applied to the build platform. This film makes it so the part adheres to the build platform throughout the print but also allows them to be removed relatively easily. This helps to minimize damage, if any occurs,

while removing the parts. An adhesion film called LithaPrime 31 was applied to the build platform. This is a liquid that is spread across the build platform and needs to be cured using a UV light.

The top of the build platform is glass because during the Adhesion Layer, in addition to the bottom LED light engine, there are also LED lights inside the build platform mount. The lights inside the mount are used to help cure slurry across the whole platform during the adhesion layer. Due to this the build platform must be transparent. Electrical tape was wrapped around the sides of the build platform to prevent light scattering though the sides of the glass. If light were to be scattered through the edges then it could cure undesired slurry in the vat and lead to issues when the wiper blade attempts to recoat the vat with slurry in between layers.

2. Post Processing

Once the print if completed, the parts have to be carefully detached from the build platform. This is done by using a razor blade and some LithaSol 20, a proprietary cleaning solution design by Lithoz GmBH to be used with alumina. Figure 3 shows alumina parts being removed from the build platform. Parts are then cleaned to remove any uncured slurry from the part using compressed air with the addition of LithaSol 20. The compressed air is used by means of an airbrush that has a siphon feed tank. Special care is taken to make sure that excess slurry is removed from tight corners and fine detailed areas. While not being too aggressive to damage the part. Printed parts need to be cleaned relatively soon following the printing process to prevent the excess slurry from drying on the parts.

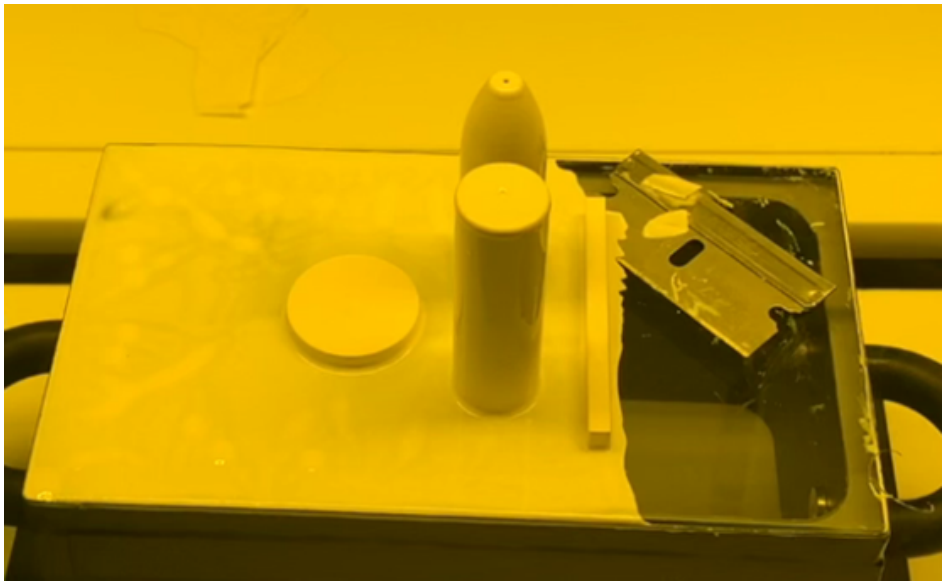

Figure 3. Shows the removal of parts from the build platform using a razor blade

Following the parts being cleaned they need to be thermally processed. In LCM, the printed part is a green body, it is relatively fragile and weak. Additional thermal processing steps are required when additively manufacturing a ceramic part. This techniques uses a photocurable organic matrix, the initially produced parts are composites that require subsequent thermal treatment[8].

When producing parts by means of LCM there is a specific multiple step schedule to thermally process the parts that is dependent on the material and the wall thickness of the printed component. During the thermal processing the part has to go through a debinding and a sintering stage. This includes being preconditioned (if needed), debinding, and sintering. For each material the wall thickness is the determining factor that dictates the specific post processing schedule that needs to be followed. As the binder needs to be removed from the parts, it is more difficult for binder to be removed from a thicker cross section compared to a thinner one. For a thick walled part it requires a slower heating profile to allow time for the binder to be removed from the part carefully so no damage occurs to the part.

Debinding is the process of removing the additives used to produce the component during the manufacturing process. In this process the organic components are burned out of the part. The length of this process is dependent on the material and thickness of the

cross section of the part is as it needs to remove the binder carefully from the microstructure of the whole part. This step of thermal processing can take multiple days if the geometry has a thick cross section to avoid cracks in the final structure[14]. The part is fragile after this process as there is no longer any binder holding the particles together. Then the part undergoes sintering, define as the consolidation of the product during firing. Implying that within the product the particles are joined together. Typically shrinkage and densification occur at this step but not always[15].

It's critical that during the thermal treatments that the temperature is precisely controlled to reduce the thermal stresses and avoid cracking from occurring in the parts[10]. For examples parts that have a wall thickness of less than 3 mm, do not have to undergo preconditioning. With that wall thickness, printed parts can be cleaned and loaded directly into the furnace to undergo debinding which would take just over 2 days for alumina using a slow heating profile. For alumina the heating profile included multiple ramp rates and dwell times. The ramp rates were very slow, most were around a tenth a degree Celsius per minute. A slow heating process is use to carefully remove the binder from the microstructure as to prevent defects from emerging in the parts. If the parts are heated too quickly and the binder is abruptly forced out of the parts it will result in the parts cracking.

Following debinding, samples are extremely delicate and need to be handled with care to prevent cracks from forming. At that stage, parts have characteristics that resemble chalk. Sample can then be sintered which for alumina takes 2 days. The parts are slowly ramped up to the max temperature, 1,650° C, where they dwell for 2 hours until ramping down to room temperature.

3. Printing Direction

With additive manufacturing of ceramics the direction in which a part is printed can affect the strength of the part. Figure 4 shows the different print directions for LCM and how they would be held in a 4-pt fixture. Even with very fine resolution, the layers can be seen throughout the part. One of the issues that can occur is delamination, the printed layers separate from each other. This can be seen by producing test bars printed in different directions and then preforming a 3-pt or 4-pt bend test on the bars. For the alumina slurry with a purity of 99.8% it can achieve a strength of 397 MPa for the x direction, 394 MPa for the y direction, and 356 MPa for the z direction[16].

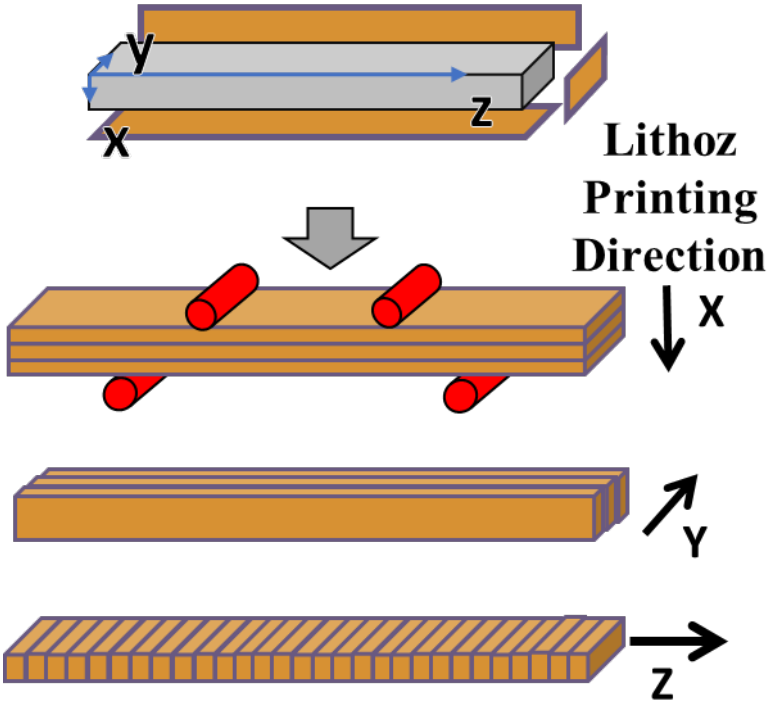

Figure 4. Different printing directions that are produced on a Lithoz's printer and illustrates how each are held in a 4-pt fixture during testing.

II. EXPERIMENTAL PROCEDURE

The process down selected for this work was LCM, which is a proprietary technique used by printers that are produced by Lithoz GmbH. LCM is a subset of Digital Light Processing (DLP). This technique is capable of producing a high strength[8], fine resolution[14], and high surface quality part[14]. The printer (Figure 5) being used is a CeraFab 8500 Research Model (Lithoz GmbH, Austria). This printer has an upgraded resolution compared to the standard CeraFab 8500. This machine's lateral resolution is 40 μm and the layer thickness can range from 25 - 100 μm. The build envelope of this machine is approximately 76 mm x 43 mm x 150 mm (L,W,H).

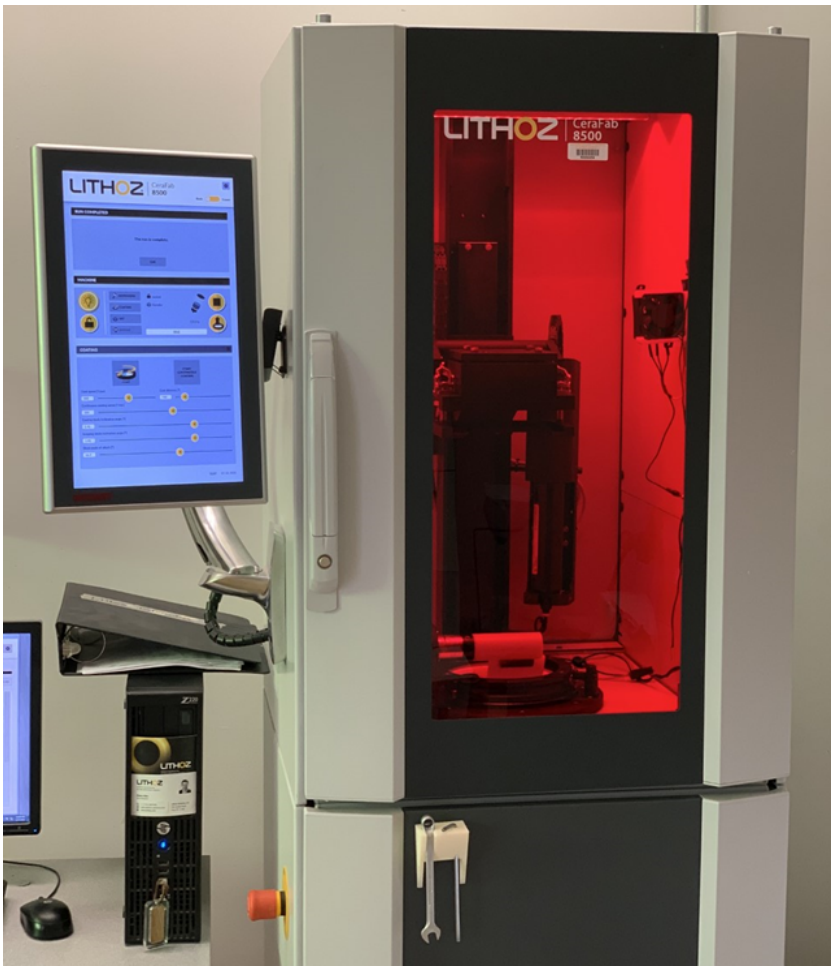

Figure 5. Lithoz CeraFab 8500 LCM printer

The plan to start with a simplified design to verify the process and make it easier to determine what attributes of the geometries are difficult to produce. The idea behind this was if a part yielded good results then the design was modified closer to the end goal adding another design element to the geometry. Along with investigating the problem to see what could be done to resolve the issue to make the feature producible. In the beginning a simplified nozzle design was used, two designs were produced to check the capabilities of the process. One problem with ceramics is the material does not like sharp points. All the corners and edges in all of the designs had small fillets on them to make them rounded. The designs worked to keep the same wall thickness, or as close as possible, throughout the part.

A. Printing Material

Lithoz offers two alumina oxide slurries, LithaLox 350 and LithaLox HP500, a purity of 99.8% and 99.99%, respectively. LithaLox 350 (99.8%) was used for this project which has a solids loading of 49 volume percent. Slurries are comprised of a photopolymerizable monomer mixture filled with ceramic powders. The photoinitiator was selected to meet the characteristics of the emitted wavelength of the LED project system[2].

The Lithoz slurry, LithaLox 350, was examined using a FEI Quanta 200 F environmental scanning electron microscope (ESEM) (ThermoFisher Scientific, USA). Images were taken to look at the particle size and to check for any contamination in the slurry. To prepare the slurry it was mixed with some DI water to help rinse the binder off of the particles to obtain a better image. A thin layer of the mixture was applied piece of carbon tape was on an aluminum metal stud. The sample was then placed in a 100°C drying oven to ensure that it was thoroughly dry.

Initially it was gold coated but it was quickly seen that charging was still an issue. The high amount of charging lead to the image being washed out and moving while trying to capture an image. Even though it was unable to capture an image it could be seen that the particles used in the slurry were very small, less than a micron. This led to an uncoated sample in Low Vacuum (Low Vac) to be used. The Low Vac environment works to minimize charging on the surface. In this mode, which has a pressure of 0.9 torr, introduces some water molecules to the environment. The water molecules absorb some of the excess

charge which minimizes charging on the surface and helps prevent the image from being washed out. Figure 6 shows one of the images that was used to measure the size of the particles.

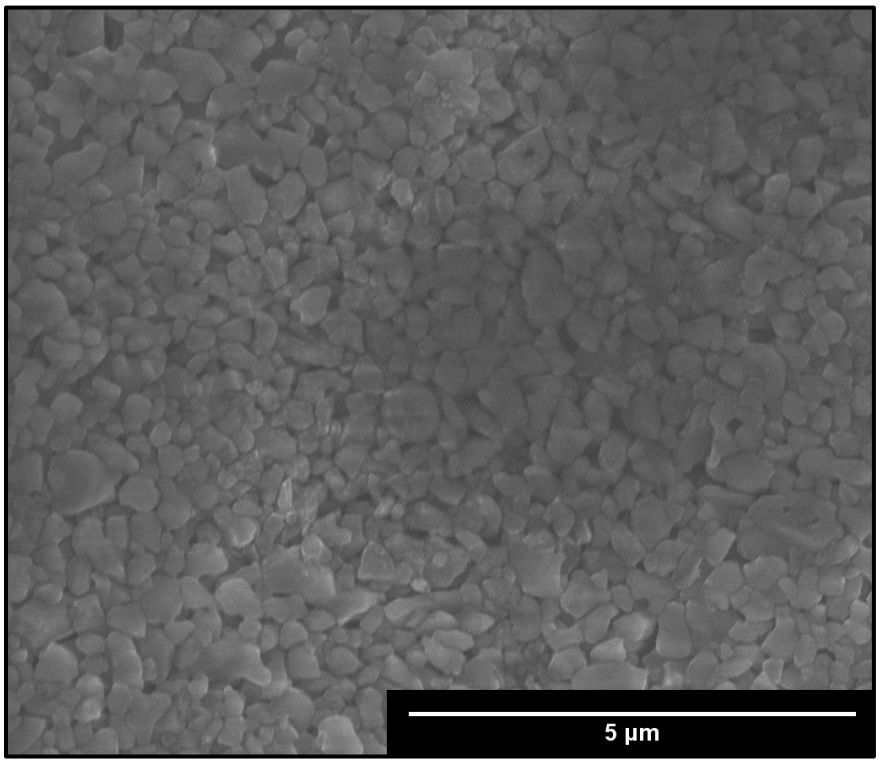

Figure 6. Alumina particles of LithaLox 350 (99.8%) mixed with DI water being observed on a ESEM in Low Vac mode

ASTM has several techniques that can be used to determine the grain size. For this work the intercept method, referred to as the Heyn method, was used. For this method a line of a known length, L_{line}, is drawn across the image and the grain boundaries that intersect the line are counted. Different grain boundaries have specific valves associated with them. A grain boundary is counted as 1, a tangent as ½, and a triple point as 1½[17]. Each image had 6 lines drawn in 4 different directions. Figure 7 shows an image of the slurry with yellow lines depicting the layout of the lines drawn on each sample. The grain size was calculated for each line and then the six calculated sizes were averaged. Resulting in the average particle size of 0.3 µm for the particles in the slurry.

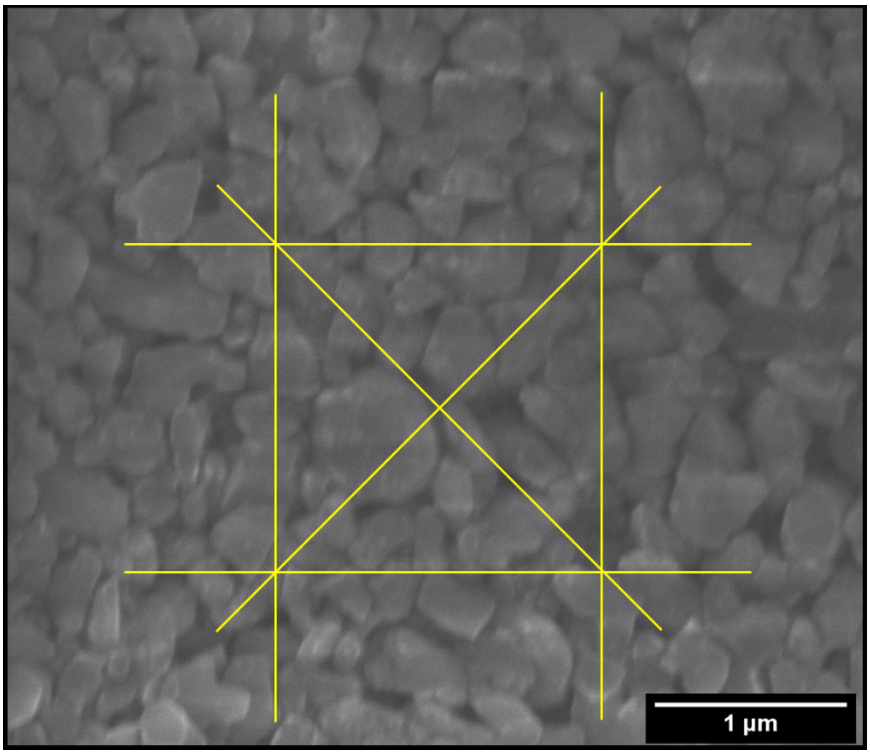

Figure 7. Lines drawn overtop of alumina particles with that represent that layout of the six lines that was used to determine the average grain size via the intercept method.

B. Producing Samples and Selecting the Geometery

This printing process yields better results when an adhesion film is used on the build platform. When printing with alumina, LithaPrime 31 is recommended. This is a liquid adhesion film that must be applied evenly across the build platform and then cured under a ultra violet (UV) light. The build platform was weighed before and after the LithaPrime 31 was applied to check that the sufficient amount was on the build platform. The acceptable range that was used was in-between 0.5 g and 1.0 g, with 0.8 g as the targeted amount. Once the correct amount was applied the build platform went under a UV light for six minutes to cure. Following being exposed to UV light a paper towel was laid on a table, and the build platform flipped over and pressed into a paper towel to remove any excess uncured LithaPrime 31. This also helped to even out any high spots on the build platform. Occasionally this process was repeated a second time if a high amount of LithaPrime 31 came off onto the paper towel.

1. First Design

When printing the nozzles, a test bar and test disk were also printed. Figure 8 and Figure 9 show the first geometries to be produced which were called “can design” and “bullet design”. These geometries had the same outer diameter and overall height. The parts are printed in the x direction with and a 50 µm print layer was used. These parts did not have any issues being printed. The first few did have some issues when they were removed from the build platform. Due to an insufficient layer of adhesion film being applied to the platform the parts stuck to the build platform. This made removing more difficult and cause some to break in where the part contacted the platform. The rest of the geometry would remain intact. When cleaning the parts, the can design took longer as the flat top perpendicular to the wall made it hard to remove the excess slurry. While cleaning the test disks it was seen that some would have indents or voids in the surface of the disk.

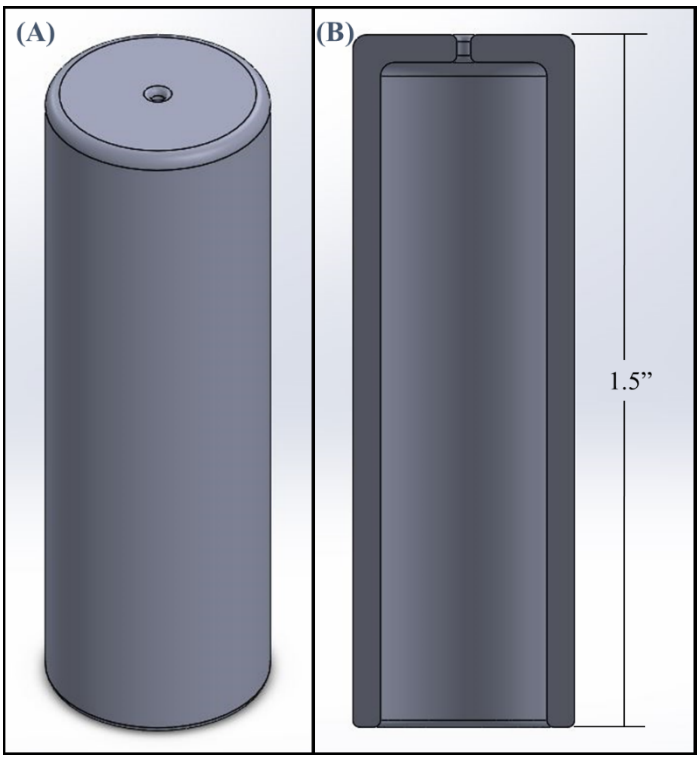

Figure 8. First version of the can design that was produced. (A) isometric view, (B) section view

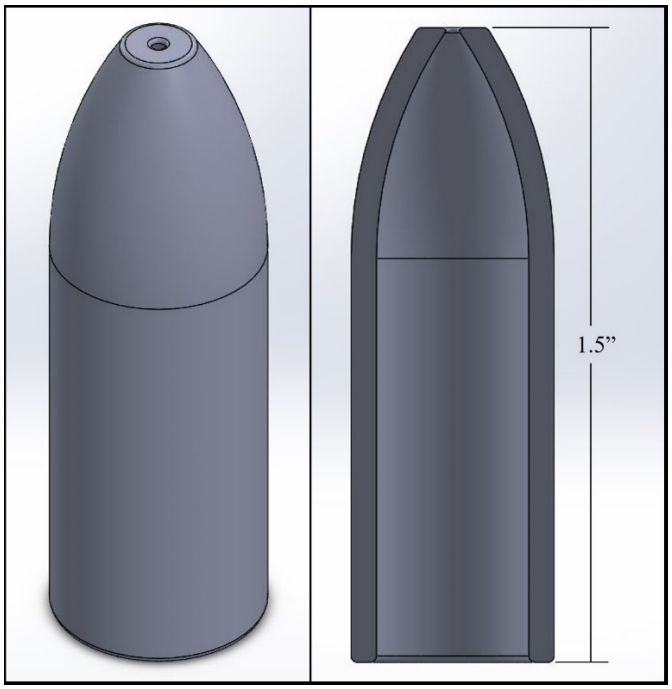

Figure 9. First version of the bullet design that was produced. (A) isometric view, (B) section view

Then parts were inspected visually for defects and no signs of defects were seen. The parts would also be inspected using a flashlight to shine light though the part to illuminate any cracks. While shining light though the part, if there was a crack or defect then a difference in the light could be seen. Inspecting parts with light was best once the parts were sintered as light is able to pass through the sintered material better. It was harder to shine light though a part that was just printed or debinded but with a bright flashlight and a dark room it would work. After the samples were checked, they went through the debinding process and checked again prior to being sintered. No cracks were seen in the parts but there was a few issues while they went through debinding. Occasionally some of the top portion of the can design, the flat top, would delaminate during the debinding process. While being removed from furnace following debinding, it would fall off. After several prints with these designs a majority of the prints come out good.

2. Second Design

The geometries were then modified, as seen in Figure 10 and Figure 11, to include a flared lip at the base of the part. The flared lip is a critical part of the geometry as that is

how the part will be held in its application. The rest of the geometry was kept the same as the first design. The parts are printed in the x direction with the flared lip based contacting the build platform. For these prints a 50 μm print layer was used.

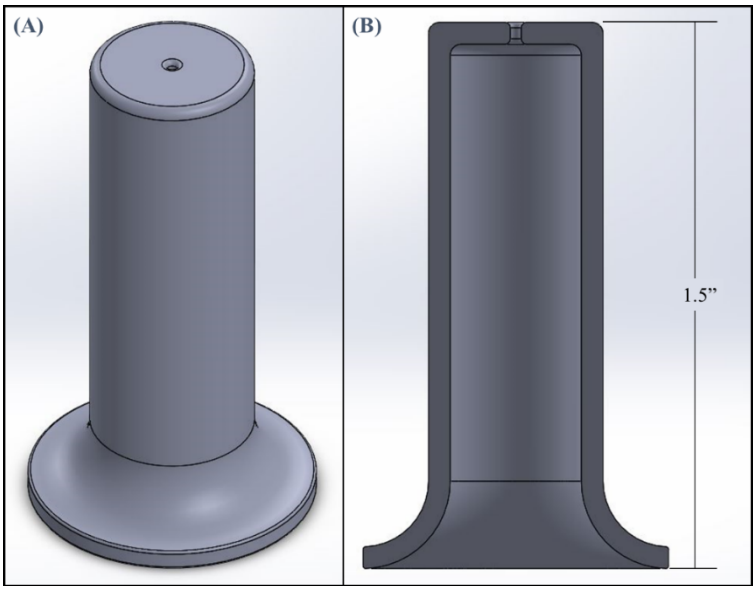

Figure 10. Second version of the can design that was produced. (A) isometric view, (B) section view

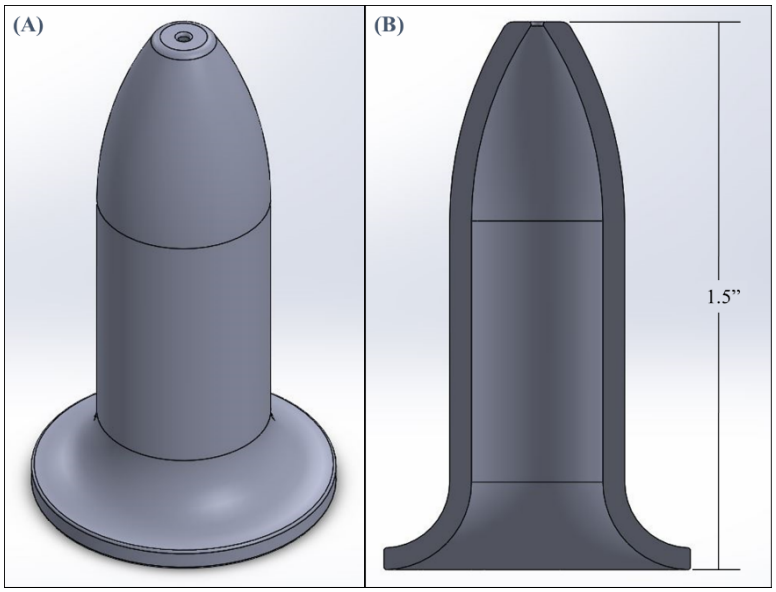

Figure 11. Second version of the bullet design that was produced. (A) isometric view, (B) section view

The first major issue with this design was with the transition area where the vertical wall transitions into the flared out lip. It could be printed with no issues but following the debinding process almost all of the parts would crack around that area. The parts that cracked would have a clean break where the curved lip meets the vertical wall. This happened with both designs, “can design” and “bullet design”, which had the flared lip at the bottom. It would only happened to parts while going through the debinding process. If a part was able to survive debinding with no cracks the parts went on to be sintered and would yield good results.

Due to this, it was determined that the issue was happening during the debinding stage. The issues with printing flared curvatures on parts is that during the debinding process the part loses the binder which until this point was holding the structure together. In the debinding firing, the parts are being heated to 1,100° C (2,012° F), this temperature burns out the organic binder but also causes the part to shrink towards the end of the firing schedule. The combination of the two results in forces being applied that the geometry that it is unable to handle causing the part to break, in order to alleviate the stress, in the curved region. With the parts resting flat on a alumina plate there are a few issues including that 1) air is not allowed to evenly flow out from the inside of the part, and that 2) as the part shrinks there are drag forces induced on the flared lip. The weight of the part acting downward on the lip and as the part shrinks it slides inward on the alumina plate.

Figure 12 shows a cross section of the printed part with arrows highlighting the forces that are acting on the geometry during the debinding. The combination of those two issues cause the part to crack at least half of the time. To resolve this issue a setter plate was designed and used during the post processing.

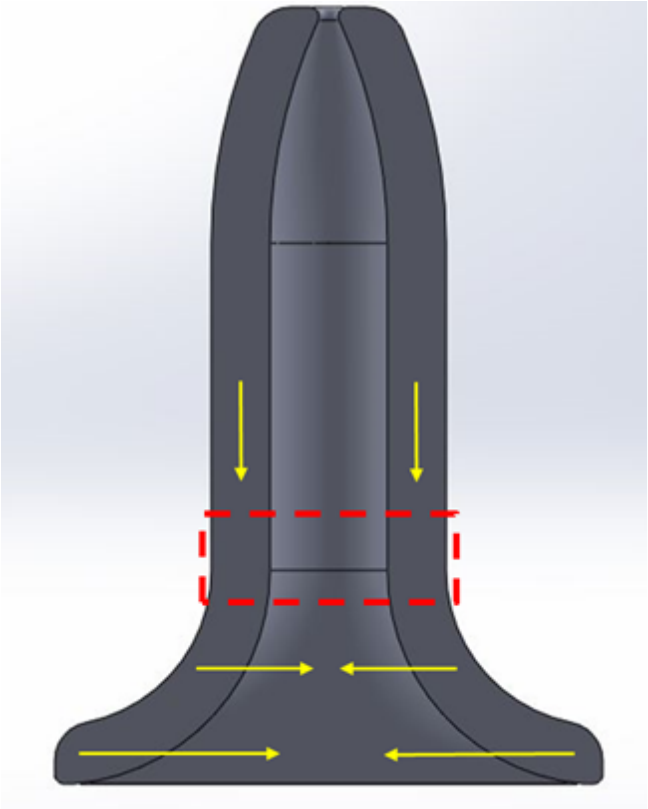

Figure 12. Shows the forces that act on the geometry during the debinding process that induce the stress causing the part to break. The red box highlights the region where the part would break.

3. Third Design

Printing of the "can design" was ceased and just the "bullet design" was used moving forward. The large flat cross section at the top of the geometry was continuing to occasionally break and the "bullet design" was yielding better results. The design was modified to be a closer size of the end goal so the part was given a smaller inside radius, shorter overall height, and slightly thicker wall. A third design was made resembling the bullet design.

There were two versions made; one had a hole in the top and the other did not. This was done so initial pressure tests could be done with the geometry without the hole to see what they could withstand. Figure 13 shows the version that included the hole at the top of the geometry. The parts are printed in the x direction with the flared lip based contacting the build platform. A 50 µm print layer was used for these samples.

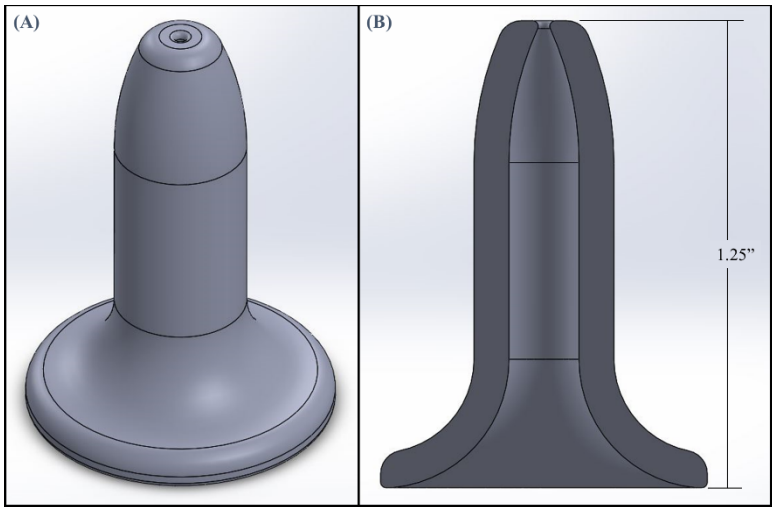

Figure 13. Third version of the Bullet Design that was produced. (A) isometric view, (B) section view

C. Non-Destructive Optical Inpsection

1. Inspecting with Light

An effective, non-invasive method of optical crack detection involves introducing light into the sample and observing the way in which the light scatters through the ceramic. It is totally nondestructive and is as fast as visual inspection. There is no sample preparation for this method and it makes it a good option to be used for screening, quality control, and failure analysis. In order to use this technique the material needs to be able to scatter light uniformly in all directions. That being said the material must also be translucent in nature otherwise this process cannot be used[18]. The technique has been referred to as "vicinal illumination"[18] because the sample is illuminated near, but not directly onto the area of interest. In vicinal illumination, light is refracted into the sample in a small area, and scatters outward in all directions. If the light encounters a crack, it is reflected back toward the source, and is not transmitted across the crack. This causes a high contrast delineation between bright and dark areas at a crack surface[18].

The light was supplied by a 10,000 lumen flashlight and was shown directly into the part. In order to only have the light interact with a small section of the part and allow the light to scatter through the part a black cap with a small hole was additively manufactured from PLA plastic. The cap was placed over the flashlight. This allowed for the light to only shine through the hole in the cap which made it more effective as to

illuminate a specific section of the part and not have the light wash out the cracks making them not visible. When the nozzle was placed upright on the flashlight, the light would only be directed into the inside of the geometry. This allowed the part to be illuminated from one side. Figure 14 shows a ceramic part being visually inspected normally and by means of illumination.

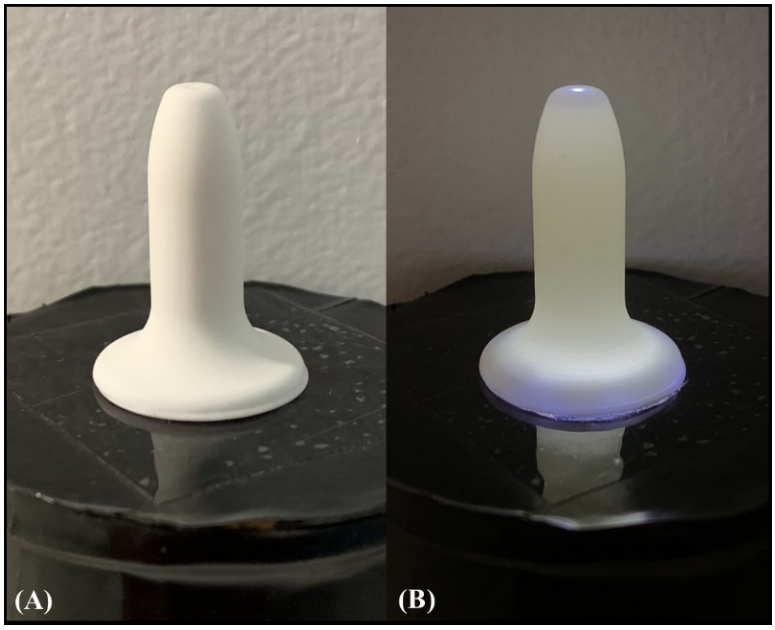

Figure 14. Shows a sintered sample on the flashlight to check for cracks. (A) normal optical inspection, (B) illuminated optical inspection

2. Inspecting with Ink

While the parts were inspected visually using light to check for cracks throughout the process, following being thermally shocked, ink was applied to help see the cracks. To apply it a KimWipe was submerged in black ink and then wiped onto the parts. The outside of the parts were coated with black ink and let stand on the parts for several minutes. They were then rinsed with DI water and carefully patted dry with a KimWipe as to not remove the ink from the cracks. The ink was only applied to the outside surface so to see if any cracks breached the wall of the part. If ink was seen on the inside of the sample then it was known that the crack was not just on the surface but broke through the wall of the part. Figure 15 is a sampled that had ink applied to it and a crack can be seen in the geometry.

Figure 16 is a sample that had ink applied following being exposed to thermal shock. It is also being illuminated to assist in seeing the cracks.

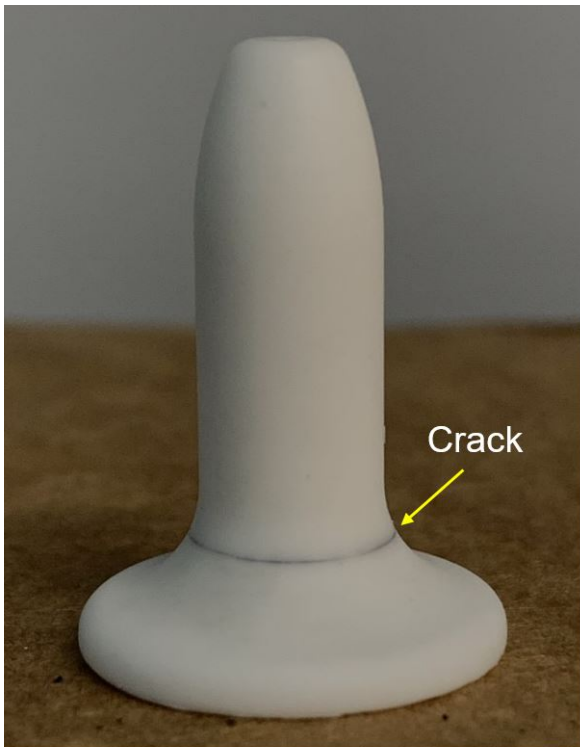

Figure 15. A sample that had black ink applied to it. The ink was able to flow into the crack near the bottom portion of the sample which allows us to visually see it.

Figure 16. Shows a sample that was thermally shocked to ΔT of 500°C and was then covered with black ink. The sample is also being illuminated by using a flashlight to better shows the cracks.

D. Correcting for Part Defects

1. Regulating the Temperture of the Print Environment

When printing began, the humidity in the room was controlled to keep it low and left the temperature at room temperature. A dehumidifier that was kept on and programmed to keep the space at or below 30% humidity at all times. Lithoz suggests the acceptable range for the printing environment is less than 50% humidity. The temperature of the printing envelope was originally determined by the temperature of the room. When printing started, it was seen that the prints would have divots in the surface of them. This was thought to be from air bubbles that get trapped when the build platform descends and contacts the vat. There tended to be a larger amounts of divots found in parts that had a large surface area, in the X and Z planes, contacting the vat. The theory is that the air bubbles are able to escape if there is a small surface area, like a 2 mm thick wall of a part, but are unable to escape from a large surface area, like a 20 mm circle. In looking to minimize the amount of air bubbles that would get trapped in the part the temperature of the print envelope was heated slightly higher than room temperature.

By increasing the temperature the goal was to lower the viscosity of the slurry, specifically in the photopolymer that was in the slurry. The higher temperature lowers the Van Der Waal forces that are acting on the molecules. By lowering the attractive forces between the molecules it increases their ability to move. The decrease in surface tension will allow for the any air bubbles that do form to move more easily among the slurry. This will give a greater probability, if any air bubbles are formed, of escaping from the cross section of the part when the build platform contacts the vat.

To determine the temperature that the print envelope should be heated to, several prints were done at different temperatures. The prints were visually compared to each other to determine the best temperature. Figure 17 shows the print envelope with the heater that was made and mounted on the middle of the side wall to heat the space. The heater consists of a Arduino microcontroller board, computer fan/heater, thermometer. Arduino is a platform of open-source electronics that produces both hardware and software. Known for being an easy to use platform which has a low cost compared to other microcontroller platforms. Arduino board is able to read inputs and turn it into an output. A mount was 3D printed to hold all the components together and make it easier to attach the unit to the wall of the print envelope. While the heater is mounted halfway up the wall to keep it out of the way during printing, the thermometer for the unit hangs lower near the vat as to make sure that the temperature of the slurry is affected. With the heater being mounted in the middle of the print envelope the fan works to circulate the air in the print envelope to make sure the whole space is heated.

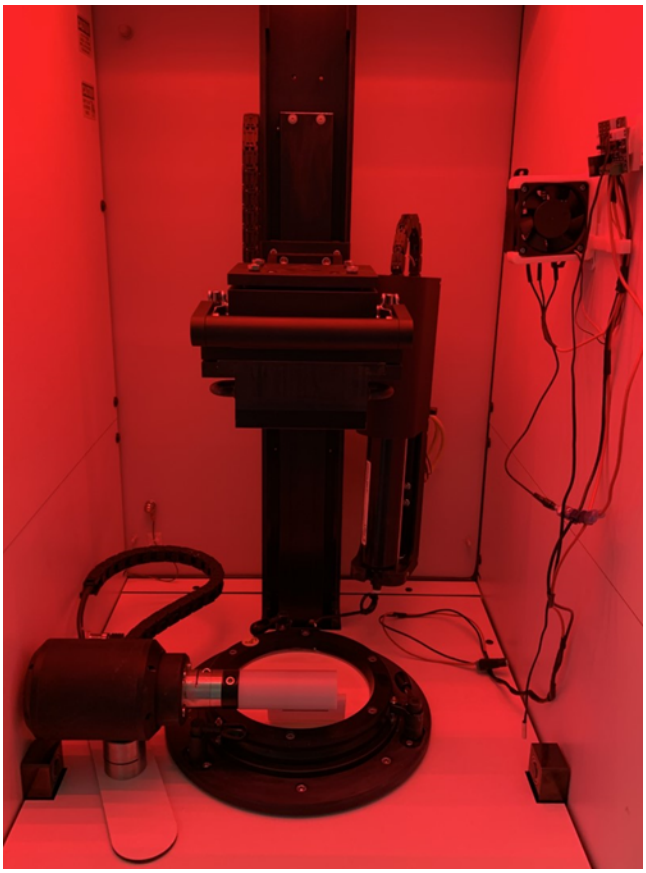

Figure 17. The print envelope of Alfred University's Lithoz CeraFab 8500 printer. The heater is mounted to the wall of the print envelope.

Five prints where done, four of them included heating the print envelope. The first print was done at room temperature, 21.1° C (70° F). To heat the print envelope four temperatures were used; 25.0° C (77° F), 26.6° C (80° F), 30.0° C (86° F), 35.0 °C (95° F). After the prints, the samples where cleaned and compared without being post processed. A large cross section part was used to compare the results of the different prints. The large cross section was effected more by the divots than smaller cross section parts. The room temperature and 25.0° C (77° F) yielded similar results. Both had divots in the surface of the disk. The remaining three prints, 26.6° C (80° F), 30.0° C (86° F), 35.0° C (95° F) yielded similar results but saw a decrease in the amount of divots in the surface of the disk. From the different temperatures that were used it was selected that 26.6° C (80° F) was a good temperature to use to print with. The higher temperatures also worked to minimize

the amount of divots in the samples but all the samples above 26.6° C (80° F) yielded similar results.

2. Using a Setter Plate

To help resolve the issue of cracking that was occurring during the debinding process a plate was designed and printed to hold the part. The plate that was designed resembles a wagon wheel, with a small circle in the middle and a larger circle around it, the two are connected by multiple spokes. Figure 18 (A) is a CAD rending of the setter plate that was produced. The setter plate is printed separate to the nozzle but during the same print. It is cleaned, just like the other parts, and the nozzle is placed on the setter plate for post processing. As seen in Figure 18 (B) the nozzle rests on the spokes which allows for air flow inside the part through the thermal treatment. With the setter plate and the nozzle both being printed it allows for them to shrink together, allowing for less drag forces to be induced on the nozzle.

Before the part was placed directly onto an alumina plate while in the furnace. While the parts were being thermally processed to remove the binder the drag forces were being applied to the part, resulting in the part cracking. With the setter plate being in contact with the alumina plate, the drag forces are now directed onto the setter plate. The setter plate sometimes breaks during debinding but this has allowed for the nozzle to survive this stage of post processing. The number of cracked nozzles has dropped considerably once these were used. The nozzle was placed on the setter plate during the sintering stage as well.

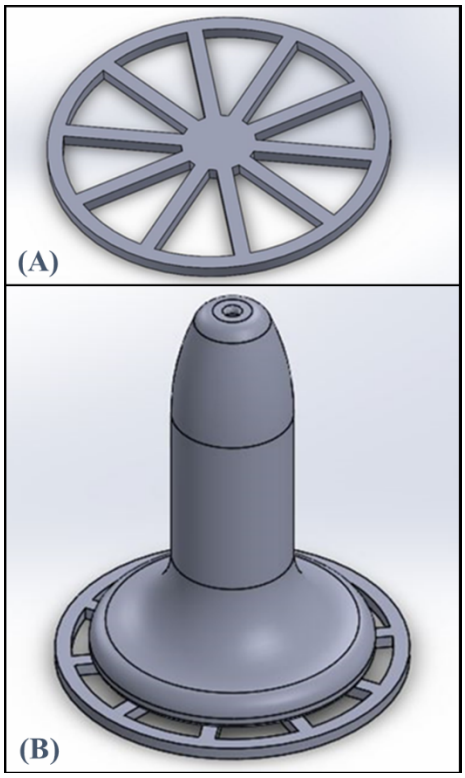

Figure 18. (A) CAD rendering of the setter plate, (B) CAD rendering of the nozzle on top of the setter plate as it will be used during the post processing

E. Testing Samples

1. Designing and Producing a Testing Jig

A major objective was to be able to apply pressure to the printed parts so in order to test the parts similar to their application to obtain some preliminary results. To approach this goal, pressure testing devices were looked at to see what systems are currently being used. This lead to the system which is used to pressure test glass bottles. Glass bottles are subjected to testing to see the internal pressure resistance of the containers. The bottles are held in place via a clamp that attaches to the top portion of the neck of the bottle. A metal tube then moves downward against the opening of the bottle. Once there is a tight seal at the opening of the bottle, the container is pressurized. Elements were pulled from those systems when designing the testing jig. The systems used for glass bottles are static as there is only one opening in glass bottles. Which is why a modified geometry was produced that did not include a hole at the top. This allowed us to test it similar to the glass bottles.

The testing jig made it so a pressure test of the nozzle could be done in order to simulate the forces it will be exposed to in their application. The parts need to experience a force on the inside acting as closely to uniform as possible on the geometry. The jig was designed to hold the part as it would be held in the real application, held in place from the flared lip at the bottom of the geometry.

For the housing part of the test jig where the part will be placed when pressure is applied; a metal electrical box that has a removable metal cover that attached by means of screws. The metal box had to be retrofitted to accommodate testing. The metal cover had a rectangle cut out of it and 4 holes were drilled at the corners of the rectangle so it would have a viewing window. That opening was then covered with 2 pieces of clear polycarbonate to provide a window to see the part during testing. The polycarbonate was attached to the inside of the metal cover via a screw, washer, and nut. This was done so it could be removed and replaced in the event the polycarbonate became damaged during one of the tests. As the box will be exposed to high pressure, relief holes were drilled on the back of the metal box. The small diameter holes were drilled along the bottom edge of the box in order to discharge the pressure.

There was a hole drilled on the side of the box to allow the pipe and mount fixture into the box. Mounting fixture and pieces of the jig that transports the pressurized air and holds the printed parts is comprised of brass fittings, brass nipples, brass ball valves, and a pressure gauge. All of the connections were threaded and had Teflon Tape applied to the threads of each joint to make sure there was a tight seal and that the joints did not leak. To test that joints did not leak a cap was attached to the mounting fixture, instead of a printed part and brass collar, and pressure was applied to the system. The pressure applied to the system was monitored to make sure there was not a drop in pressure form a leak. In addition, Snoop® Leak Detector was applied to each of the joints to confirm that the connections were sealed and did not leak. If Snoop® was applied and a leak is detected a sustained bubble action would occur at that site to show there is a leak.

Figure 19 is an exploded view of how the nozzle is held during testing. It is composed of a right angle brass fitting, tapered rubber washer, rubber o-ring, and a cap. A hole was drilled in the cap to allow for the body of the geometry to pass through but then catch on the flared lip. The hole was slightly larger than the diameter of the body to help

disperse the force to more area of the lip. For this test jig a rubber flared washer and o-ring was used to provide a seal between the ceramic and metal. The flared washer was in contact with the underside of the flared lip to provide a seal on the bottom of the geometry. An o-ring was placed on the topside of the flared lip to provide a seal on the top of the geometry.

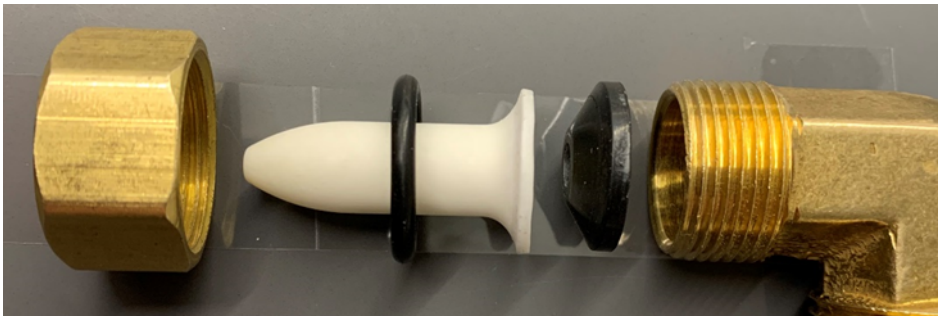

Figure 19. An exploded view of the parts used to secure the nozzle during the pressure tests. From left to right; brass collar, rubber o-ring, ceramic nozzle, flared rubber washer, and brass base.

Initially the jig was manually operated using a high pressure three stage hand pump supplied the pressurized air and a ball valve. The ball valve had to be manually opened to allow the pressurized air to reach the printed part. This worked at the beginning but the test setup was soon modified to increase the rate of testing and to have the ability to test the part in a burst mode which is closer to what the geometry will experience in the actual application.

The one ball valve was replaced for a 2-way normally closed solenoid valve. This change allows for faster, more consistent burst testing. This change also required the method in which air was supply to be upgraded in order to deliver air at the desired rate and pressure. To supply the pressurized air needed to conduct the tests a tank of industrial grade nitrogen, which are pressurized to 17.2 MPa (2,500 psi), was used. In order to discharge the air at the rate and pressure that was desired a high pressure, high delivery regulator was used. It was able to discharge the air consistently at pressures of 3.4 MPa (500 psi) and 6.9 MPa (1,000 psi). Nitrogen gas was used as it is an inert gas.

In order to better control the solenoid valve an Arduino was added to the system to operate the valve. Figure 20 shows the testing apparatus after the Arduino and solenoid

valve was added to the system. The Arduino acts as an electronic switch that allows for the power to be supplied (or not supplied) that is required to operate the solenoid valve. Arduinos are only able to supply a low amount of power to their components. Due to this a trigger switch drive module and a separate power supply had to be connected to the electronic system in order to provide the necessary power needed to operate the solenoid valve. The Arduino is wired to the external trigger switch drive module and controls when the trigger switch is on or off. This switch is component that supplies the power to the valve and allows it to operate.

The program can be written to keep the valve open (or closed) for any amount of time and for as many cycles as desired. For our tests, it was programed to open/close 10 times and at the end to remain closed. The valve would open, remain open for 1 second, then close, remain closed for 1 second, and repeat the cycle for a total of 10 times. After the tenth time the valve would stay closed.

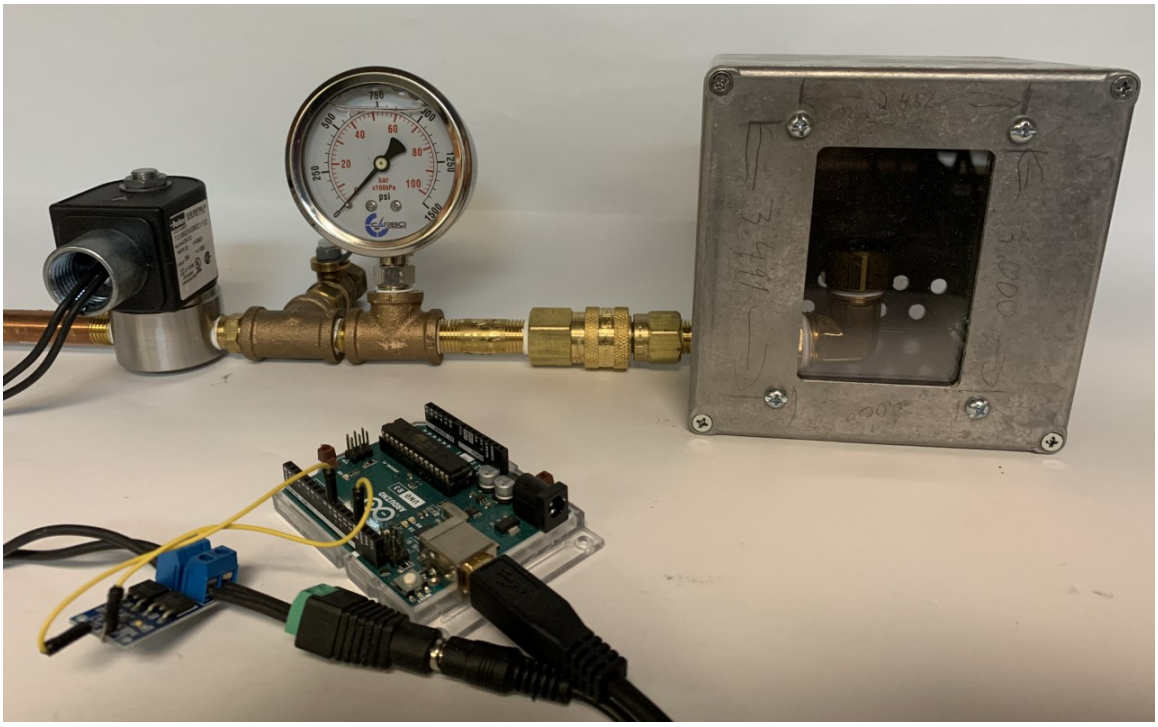

Figure 20. The final version of the testing jig that was used to pressure test the ceramic parts. The setup includes a solenoid valve, pressure gauge, metal enclosure with viewing window, and an Arduino.

2. Pressure Tests Early On

There were two versions of the third design produced where one had a hole on the top and one did not. The first pressure tests used the geometry that did not have a hole in the top. This was done to see if the nozzle was made into a closed pressure vessel what pressure it could withstand prior to breaking. The part was loaded into the test apparatus.

For the first version of the test setup there was a ball valve that needed to be closed in the middle of the test jig to allow us to build up pressure. Using a high pressure hand pump, pressure was built up in part of the testing system. For this series of tests the starting pressure applied to the part was 0.7 MPa (100 psi) and was held at pressure for 1 minute. Pressure was increased by increments of 0.7 MPa (100 psi) until 6.9 MPa (1,000 psi) was reached and at each pressure increase the part was held, at that pressure, for 1 minute. The same part was tested multiple times and did not sustain any damage.

Each sample was visible inspected, using a flashlight, to check for damage. With slow pressure tests not causing the part to fail, rapid pressurization was done to the part to see that if the part was quickly put into a tensile state if that would cause the part to fail. Again the part was held briefly at pressure to see if there would be a delayed failure. Following testing several samples, the geometry was then switched to the version that had a hole in the top.

The testing set up was upgraded to allow for the rapid pressure tests and the same tests were done. This was done by adding a solenoid valve, Arduino board, and tank of industrial grade nitrogen to the testing set up. The parts would now be rapidly pressurized which is closer to how they would be used in their desired application. This allowed for the samples to be tested more. To start this stage of the testing, it was set to pressurize the samples 15 times. Tests were done in quick succession of each other. The Arduino was set to open the valve for 1 second then close for 1 second and repeat this 15 times. Later the parts were tested for a total of 200 cycles or failure, whichever came first.

3. Thermal Shock

The parts being produced for this work will experience a force on the inside of the geometry coming from pressurized gas. Compressed gas will be forced inside the chamber which means the part will be experiencing a tensile force. Ceramics excel at being able to handle compressive forces but usually struggle to withstand high tensile forces. Alumina

also has a relatively low thermal shock resistance. Alumina is able to withstand a temperature difference of 235° C[19]. Typically if the material is exposed to a higher temperature difference, then the cracks that form will break the through the cross section of the part and lead to catastrophic failure. Ceramics are a brittle material so when they break it will be a catastrophic failure.

Ceramics are able to handle extremely high temperatures, temperatures that other materials are unable to withstand. The favorable properties are a result of the atomic bonds and crystal structures[20]. While they have excellent strength at high temperatures they struggle to handle a sudden transient temperature change or thermal shock[21]. By having strong covalent and ionic bonding this restrains the material from substantial plastic deformation, resulting in the inability to relieve stress forces and produces crack propagation[22]. While the structure of ceramics gives the material some desirable traits, it also results in undesirable traits like being brittle. As a result of this the material has little tolerance for withstanding a sudden temperature gradient[23]. This trait renders the material prone to catastrophic failure when the material experiences thermal shock[24, 25]. Catastrophic failure gives rise to a major roadblock that prevents the material from being used in certain applications.

In general the overall strength of the material is proportional to the flaw size[26]. The Griffith Theory says that the existence of flaws, in the forms of micro-cracks, explains why the actual strengths are lower than the theoretical strengths[27]. This is due to the idea that polycrystalline materials would contain flaws and elevated temperatures would cause the flaws to grow[28]. If the flaw exceeds the grain size it would impact the mechanical properties of the material[29].

For Al_2O_3, which excels at withstanding extremely high temperatures, a sudden and rapid change in temperature it typically results in critical damage. Alumina, compared to other ceramics, has a low threshold for the thermal shock it can tolerate. It has been shown that strength of alumina samples, which have been quenched in water, abruptly decreases at a temperature difference of just 300° C. Alumina samples that have not been exposed to thermal shock show flexural strength show values of 285 MPa while once they were exposed to a thermal shock of 300° C the flexural strength drops to 150 MPa[30].

The anisotropy of thermal expansion in Al_2O_3 results in residual stresses which became larger and more non-uniform. This results in cracks easily propagating across surface[28]. This highlights that temperature difference of just 300° C causes severe damage to the material[30]. While grain size alone is not a controlling factor, it has been seen that in Al_2O_3 increasing grain size can increase the fracture toughness[28]. However the amount of empty space between the grains must also be considered as minimum porosity results in improved fracture toughness[31].

To help determine a materials resistance to thermal shock Hasselmann has a equation that output a valve which can be compared amount to different materials. Equation 1[32] is a variation of the Hassel equation which was used to calculate the resistance of alumina for thermal shock. It uses four valves thermal conductivity (λ), mean bending strength (σ_B), coefficient of thermal expansion (α), and modulus of elasticity (E) to form a valve that depicts a score for the material. For alumina a valve of 4.2 is calculated.

$$R_S = \frac{(\lambda * \sigma_B)}{(\alpha * E)} \quad (1)$$

The application for the printed parts will have them experiencing an internal pressure while also going through a temperature difference. Each sample was thermally shocked and then pressure tested to see how the thermal shock will affect the parts ability to handle internal pressure. ΔT is being defined as the difference in temperature between the furnace temperature and the temperature of the quenched medium[33]. Samples were thermally shocked to four different temperature differences; 300° C, 500° C, 700° C, 900° C, respectively. The samples were heated in a muffle furnace to the selected temperature and dwelled at the desired temperature for 30 minutes. Parts were heated from the outside in and evenly across the geometry.

After being heated in a muffle furnace, they were cooled by submerging it in room temperature DI water. To achieve the temperature differences the temperature of the DI water, that the samples were going to be submerged in, was measured and that value was added that to the desired temperature difference to determine the valve that the furnace needed to be set to. The samples were loaded into the furnace in the upright position. The

furnace heated to temperature with a ramp rate of 5° C/min. Once it reached the desired temperature it dwelled for 30 minutes to make sure the parts were thoroughly heated. After the dwell period, samples were removed from the furnace using tongs and submerged in a bucket of DI water. The top of the geometry contacted the water first, and parts remained in the water for several minutes before being removed and dried.

III. RESULTS AND DISCUSSION

After parts were thermally shocked they were internally pressurized using industrial grade nitrogen. The samples were loading into the test fixture and were pressure tested at 3.4MPa (500psi), new samples were tested at 6.9MPa (1,000psi).

A. Characterication of Samples

1. TGA

Using a thermoanalyzer Q600 SDT (TA Instruments, America), thermos gravimetric analysis (TGA) was used to determine the temperature at which all the organic binder was removed from the sample. By being able to measure the weight loss of the sample as it was heated, the temperature at which the organic binder was fully removed from the printed part could be found. Normally a slow heating profile is used to allow the binder enough time to escape without causing it to crack. Cracking was not a concern for these tests so the normal debinding schedule was not followed and instead a ramp rate of 10° C/min was used. While the normal debinding process only goes up to 1,100° C for these tests using the TGA the sample was heated to 1,200° C in order to see if anything happened around 1,100° C. As seen in Figure 21 at low temperatures, less than 200° C, not much of the organic binder is removed from the material. The bulk of the reduction of weight occurs between 200° C and 400° C. With the data collected shows by 600° C all the organic binder was removed from the sample.

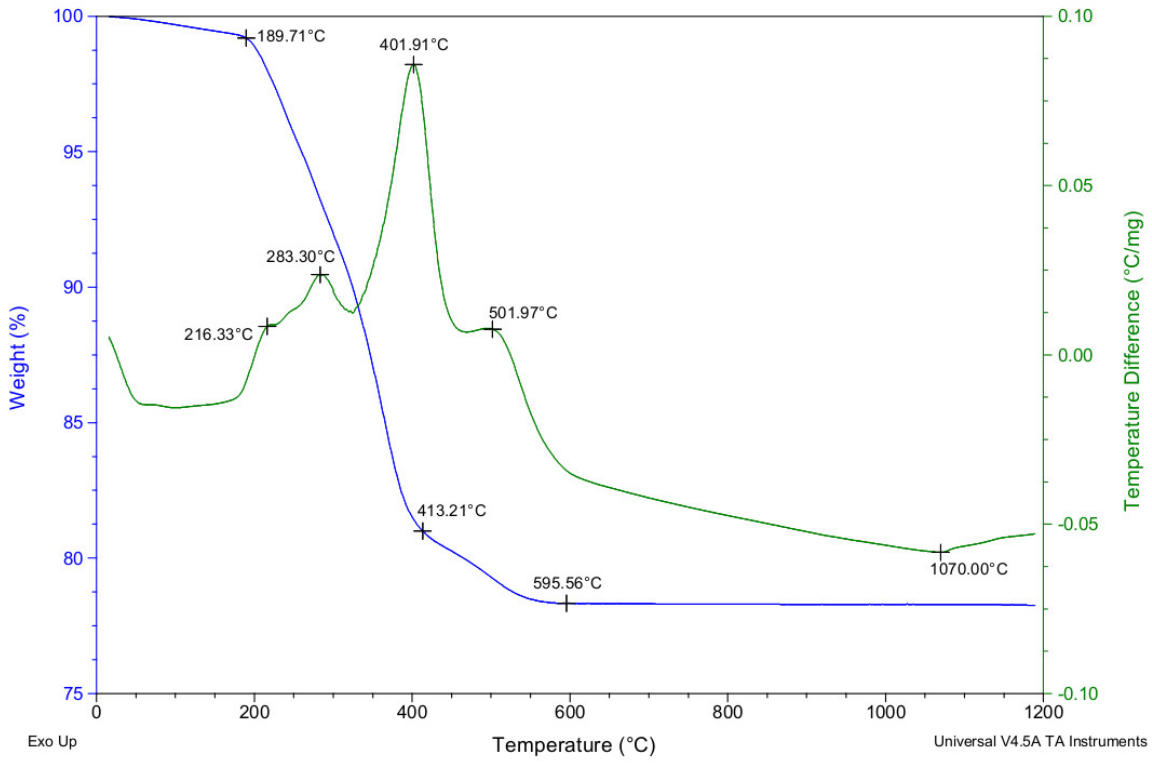

Figure 21. TGA data showing the reduction of weight, and therefore the removal of organic binder, of a printed piece from LCM

2. Examining Microstructure

Test disks were printed in order to compare the particle size throughout the process of producing the parts; preconditioning, debinding, and sintering. In order to look at a sample using an ESEM the sample must be dry so the one printed test disk needed to be dehydrated. While the printed samples did not undergo preconditioning the one test disk did to ensure the disk was thoroughly dried before going into the ESEM. The part was slowly heated to 120° C and dwelled at that temperature for 2 hours. The second and third test disk went through debinding, using the same schedule that was used for the other printed parts. The debinding schedule takes just over 2 days and slowly ramps up to 1,100° C. Once it reaches that temperature it slowly returns to room temperature. During the debinding stage, the samples were covered with a alumina crucible. Just the third test disk was sintered. The sintering schedule takes 2 days and slowly ramps up to 1,650° C. It

dwells at that temperature for 2 hours before returning to room temperature. During the sintering the part was covered with an alumina crucible.

After all 3 samples were thermally processed, they were mounted to a piece if a glass slide using double sided carbon tape. The sample was loaded into the Cressington Sputter Coater 108 (Cressington, England) and were gold coated. During that process a vacuum is pulled and backfilled with argon gas to help ensure an even layer is applied to the surface of the sample. These samples were coated for 30 seconds. During this process the sample that just went through debinding was chalk like and fragile. While attempting to gold coat the sample it delaminated. Most of the disk separated from the carbon tape but a thin layer remained intact on the carbon tape.

The microstructures of the samples were imaged under high vacuum conditions in the SEM. The sample that was preconditioned was looked at using a potential energy of 15 kV. Figure 22 show that the particles were small, less than a micron, along with some binder surrounding the particles. Binder meaning the photopolymer that was used to cure the layers together throughout the printing process which was not burned off yet. While the sample looks level an indent can be seen in the image. This indicates that there could be other small voids throughout the sample or in-between the layers.

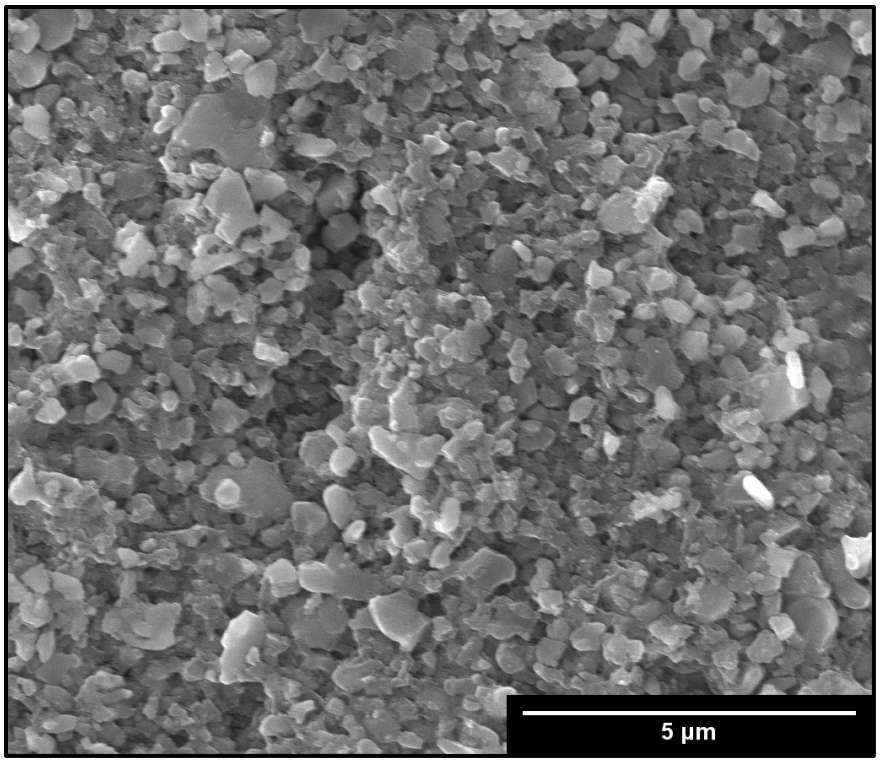

Figure 22. LCM printed Al_2O_3 sample after being cleaned to remove excess slurry and dried in drying oven

The debinded sample, which has been gold coated, had extreme amounts of charging on the surface which prevented images from being taken. As a result part of the non-coated debinded sample was mounted and reexamined without being gold coated. This time a potential energy of 25 kV was used. The higher potential allowed the electrons to blow through the top layer of the sample and reduced the amount of charging that occurred at the surface. Charging can still be seen in the image but it was a reduced amount that allowed for images to be taken. Figure 23 shows that there is no longer any binder surrounding the particles as it was burned off during the thermal treatment. Multiple small indents can be seen throughout the image. While a majority of the grains are tightly packed together some porosity can be seen throughout the grains.

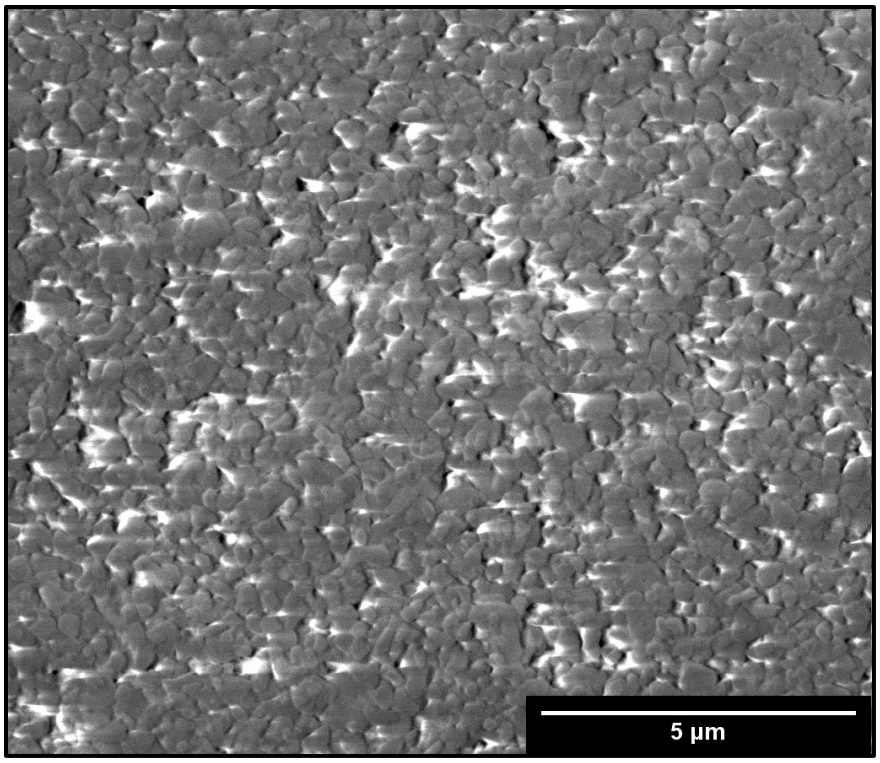

Figure 23. LCM printed Al 2O3 sample after going through the debinding stage where it was heated to 1,100°C

The sintered sample contains particles that are substantially larger than the starting size of the particles. The slurry contained particles that was less than a micron while in the sintered sample they have grown to an average size of 2.4 µm. This sample was heated to 1,650° C and dwelled at that temperature for 2 hours, just like the samples that were pressure tested and thermally shocked. Due to the high temperature of the firing the grains, as seen in Figure 24, grew a large amount. The amount of porosity among the grains at this stage has decreased compared to the debinding stage.

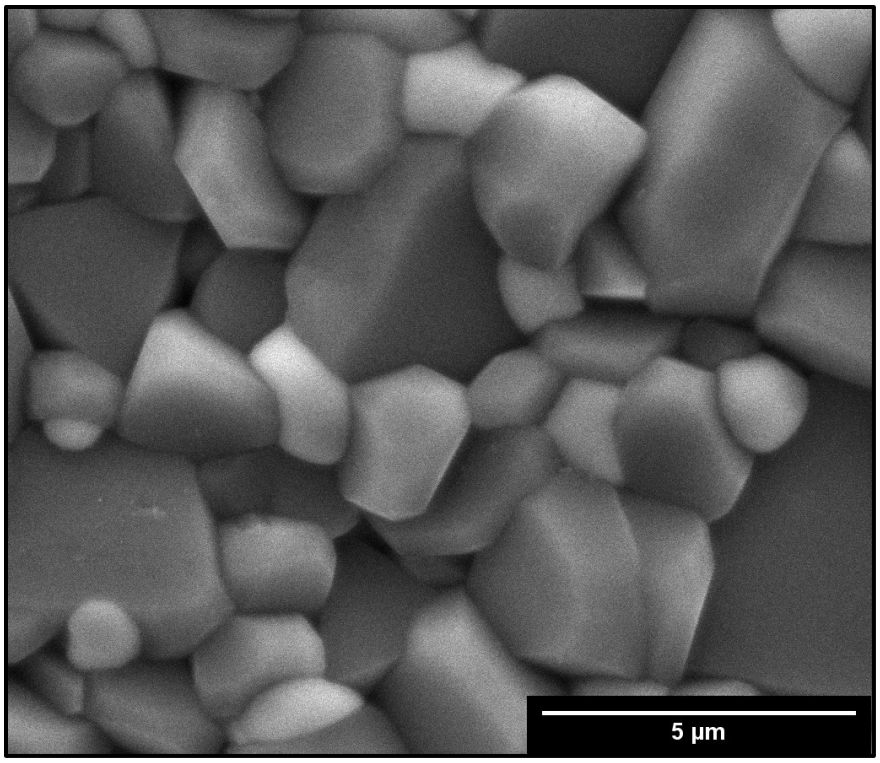

Figure 24. LCM printed Al 2O3 sample after being sintered where it was heated to 1,650°C and dwelled at temperature for 2 hours

The debinded sample shows an average grain size of 0.4 µm and they ranged from 0.31 µm to 0.42 µm. The sintered sample shows an average grain size of 2.4 µm and they ranged from 2.0 µm to 2.9 µm. Due to the high firing temperature, 1,650° C, of the sample during the sintering process it is not a surprise that the grains have grown in size.

The fracture surface of the broken samples were examined using the ESEM (Figure 25,Figure 26,Figure 27) to see if there was any variation in the microstructure of the sample. With the higher ΔT samples experiencing more cracking, which could be visual seen, it was believed that those samples' microstructure would show more fractures compared to the samples that did not experience thermal shock. In order to obtain a fragment of a non-thermally shocked sample, one was broken my means of a hammer. A piece of each of the samples were examined and while looking at the crack surface no difference could be seen, as the microstructure was similar in the three samples.

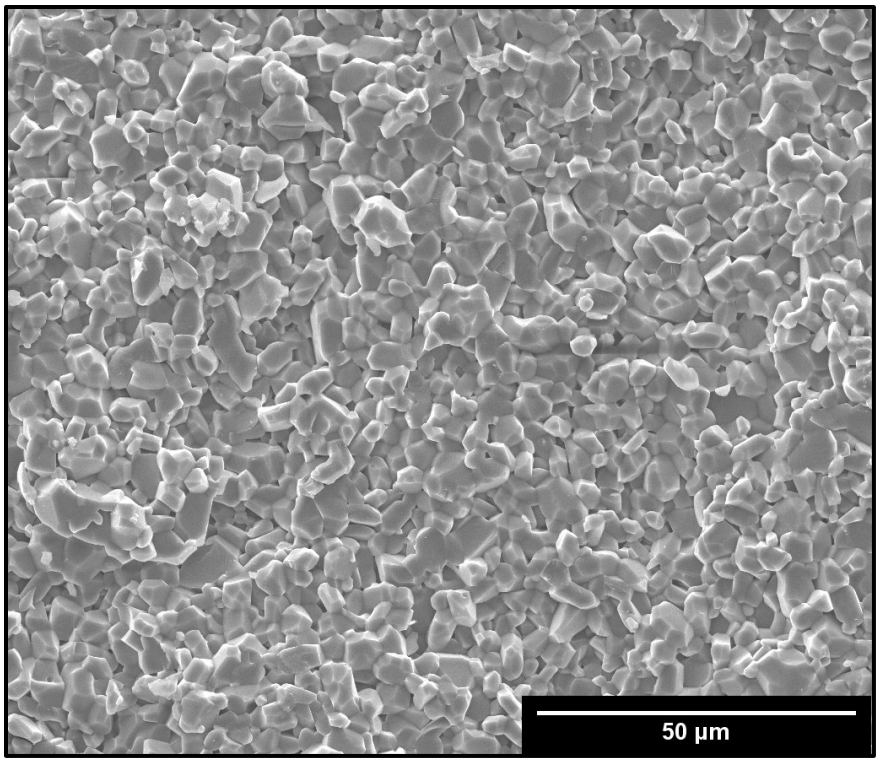

Figure 25. Crack surface of a sample that did not undergo thermal shock

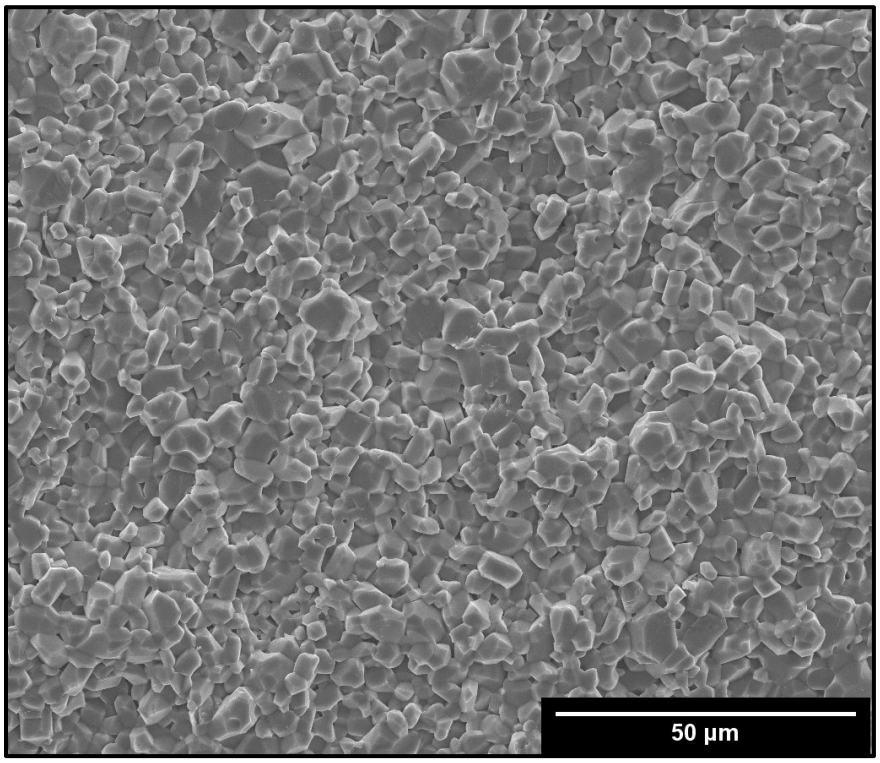

Figure 26. Crack surface of a sample that experienced a thermal shock of ΔT of 700° C

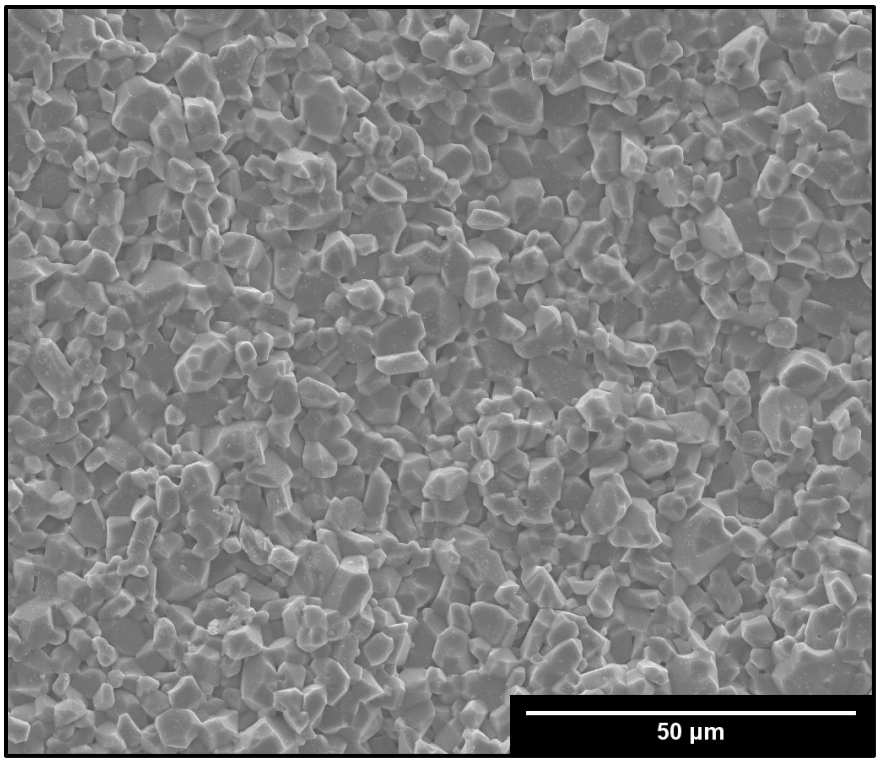

Figure 27. Crack surface of a sample that experienced a thermal shock of ΔT of 900° C

B. Pressure and Thermal Testing

The use of the printed setter plate, to support the desired geometry, provided a solution that resolved the issue of cracking that occurred during the debinding stage. The setter plate was able to absorb the stresses that are induced onto the printed parts while the organic binder was being removed. This made it possible for crack free parts to be produced, thus allowing for pressure tests to be completed on the printed samples. Pressure testing was done on samples that were not thermally shocked. Samples were able to survive pressure tests of 6.9 MPa (1,000 psi) for over 200 cycles and no damage could be visually seen on the parts.

Thermally shocking samples resulted in extensive cracking across the whole part. It was hard to initially see the extent of that damage that was done even with the flashlight. The use of the black ink allowed us a way to visually see a majority of the cracks that were formed from the sudden change in temperature. Each of the ΔT's that were tested, 300° C, 500° C, 700° C, 900° C, produced cracks on the geometry but the degree of the damage

varied. All of the samples showed a similar crack pattern even though they were exposed to different temperatures which resembled a tight grid pattern. Some of the samples had sections on the middle of the part that showed a lower amount of cracks. This was caused by the tongs that were used to move the samples from the furnace to the water. The part was held until it was fully submerged in the water when it was then released. Those sections that were covered by the tongs did not experience the extent of being thermally shocked which is why there is a decreased amount of cracks.

The samples were coated with black ink as a preliminary test to see the damage the parts obtained from being thermally shocked. The difference seen in the samples was the size of the crack opening and it was highlighted by the ink that was applied to the samples. Samples of 300° C had faint black lines across the sample. This is due to the cracks being shallow in depth and width. Only a small amount of black ink filled into the cracks as they did not have a large volume. As the temperature difference increased the cracks were noticeably darker and had thicker lines. With the increased temperatures they resulted in a wider crack opening that allowed for more ink fill in. While the 700° C samples had darker lines then the 500° C, there wasn't a big difference in the appearance of the cracks of the 700° C and 900° C.

While there was a tremendous amount of micro cracking on the outside of the geometry, not all of the samples had cracks that breached the cross section of the wall as the ink was applied to only the outside of the geometry. For samples that had a ΔT of 300° C and 500° C, the dye could not be seen on the inside of the sample. This means that cracks did not breach through the wall of the sample. The cracks were just on the surfaces of the samples that were in contact with the water. For samples that had a ΔT higher than 500° C, dye could be seen on the inside of the geometry. This showed that the thermal shock resulted in stress that was too great for the material to handle and produced a crack that broke through the cross section of the wall. This informed us that the sample already had critical flaw prior to being pressure tested.

After being inspected with ink, the samples were tested to see if they could withstand internal pressure. To start 3.4 MPa (500 psi) was applied to the geometries, beginning with the low ΔT and working up to the higher ones. For the 3.4 MPa (500 psi) the samples that had a ΔT of 300° C and 500° C survived being pressure tested 205 times

in quick succession. Samples that had a ΔT equal or greater than 700° C did not survive and were unable to handle being pressurized at all. They broke immediately upon pressure being applied to them. This shows that a ΔT equal to or greater than 700° C imposed too much stress on the geometry. Leading to catastrophic failure upon a tensile force being applied.

This same procedure was then repeated with 6.9 MPa (1,000 psi). The samples that had a ΔT of 300° C were able to survive the pressure tests. Those parts survived 205 pressure tests in quick succession of each other. The samples that had a ΔT of 500° C was able to handle some pressure tests but during the ninth test broke. The increased amount of pressure was too much for the parts to handle. The same results were achieved for the ΔT equal to or greater than 700° C as that of the 3.4 MPa (500 psi) tests. The samples broke immediately upon pressure being applied to them. Table 2 shows the results from each of the tested samples.

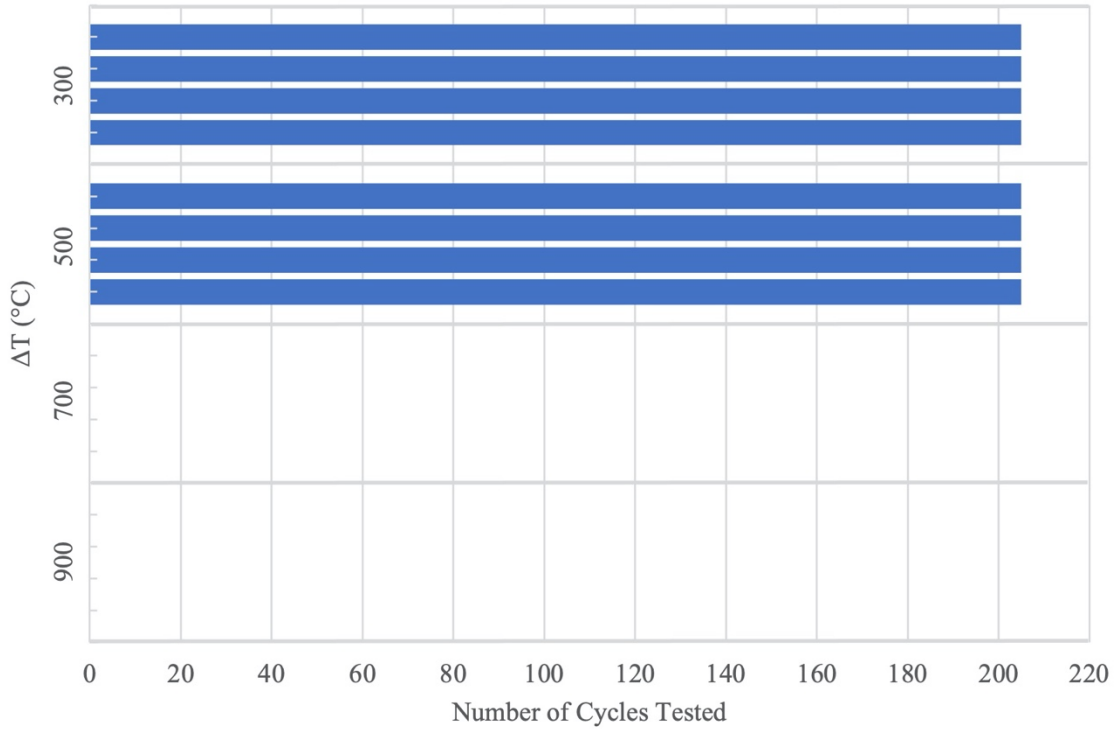

Figure 28. Shows the number of times that each of the different thermally shocked samples survived being pressurized to 500psi

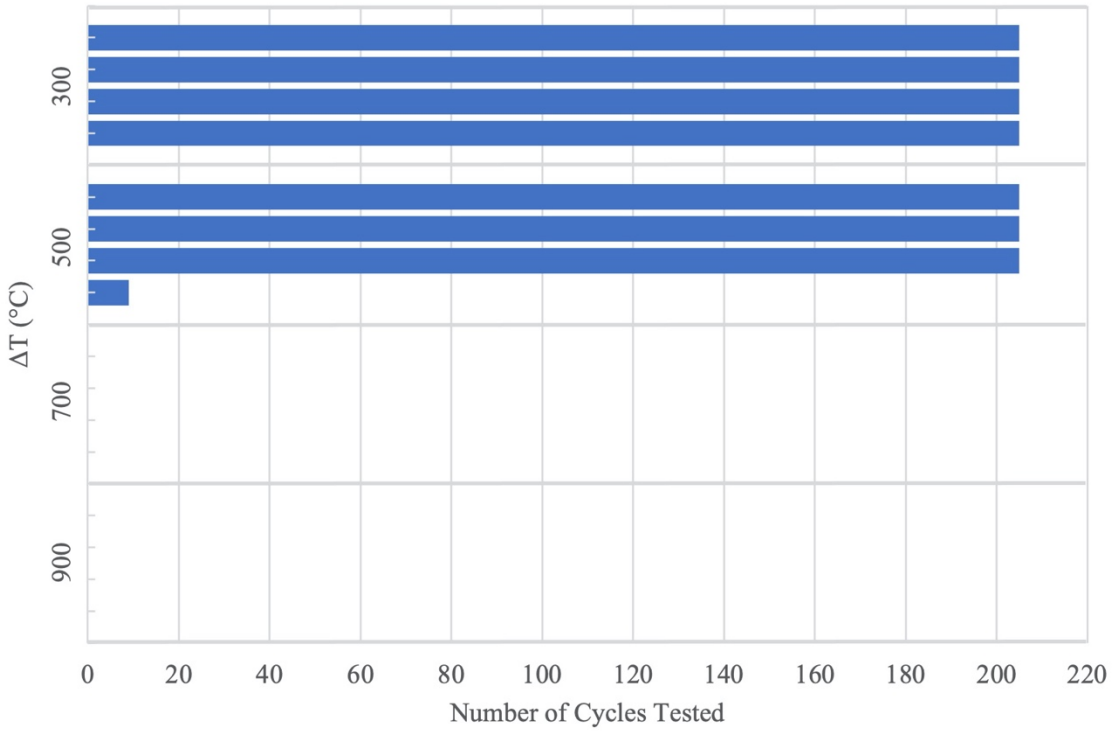

Figure 29. Shows the number of times that each of the different thermally shocked samples survived being pressurized to 1,000psi

The microstructure of the ceramic samples that broke during the pressure tests were examined on the SEM. In order to compare the broken pieces that were thermally shocked to a sample that did not experience thermal shock, a ceramic part was broken with a hammer. One of the broken pieces was mounted to an aluminum stud using carbon tape and coated with gold. For each ΔT, the fracture surface (Figure 30 (A)) and outside of the printed surface (Figure 30 (B)) were examined.

When comparing the microstructure of the printed surface (Figure 31) a difference in the grain size could be seen across the surface. In the sample that had no ΔT the grains are similar in size with only a few outliers that are larger. It is seen that as the ΔT is increased, the amount of large grains seen in the samples increased. While this was seen while looking at the printed surface it was not prominent in the crack surface (Figure 31) samples. Throughout the crack surface the grains were uniform in their size.

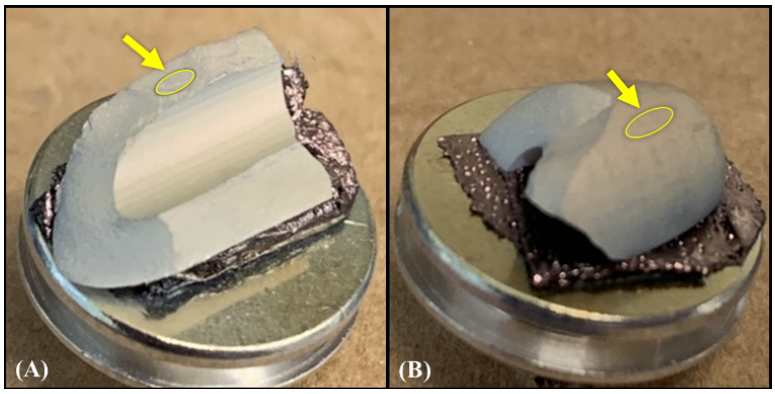

Figure 30. Defining the terminology and highlighting the region that was examined on the broken pieces. (A) fracture surface region, (B) outside of the printed surface

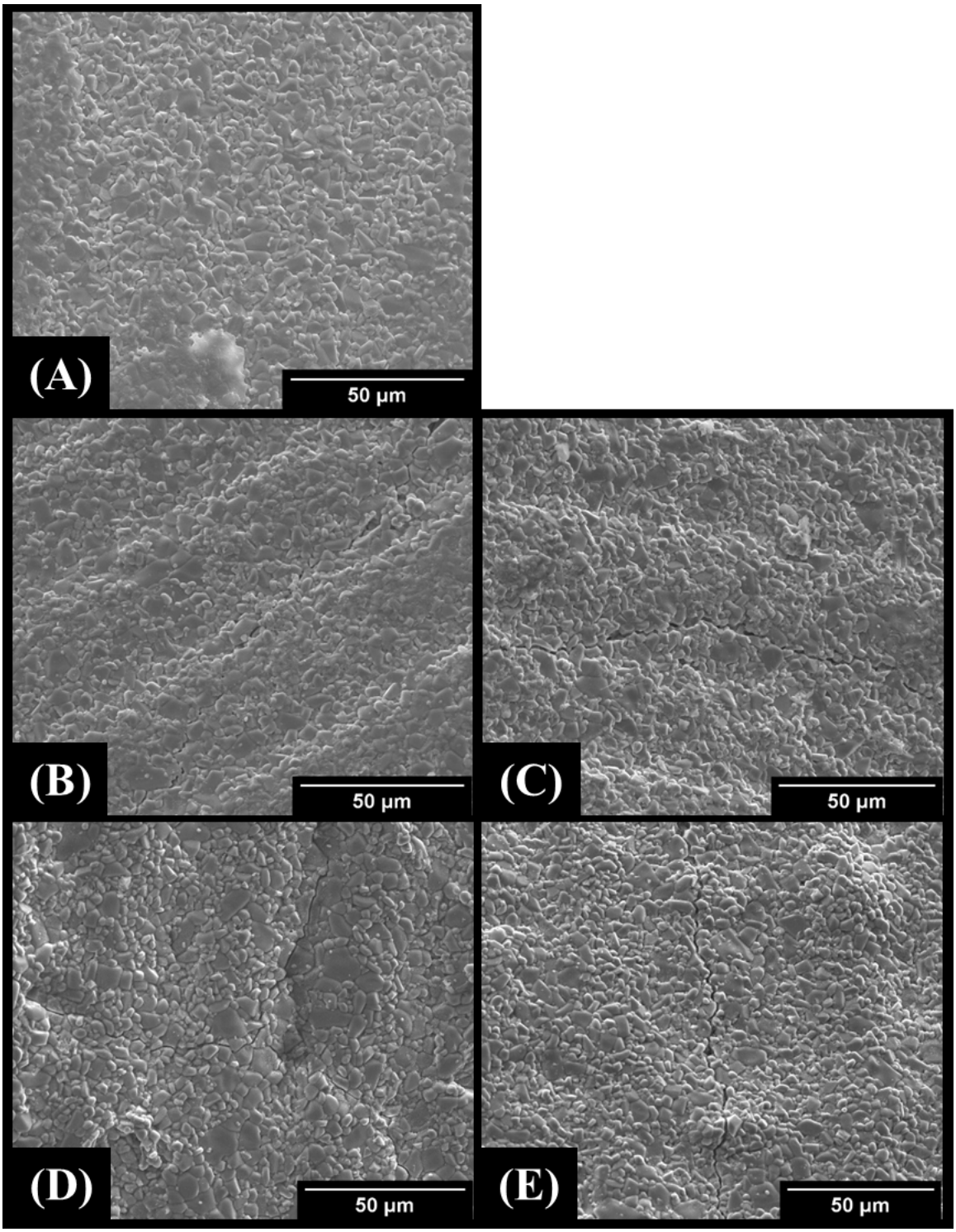

Figure 31. (A) Surface of a printed part that was manually broken and experienced no ΔT. (B) and (C) are surfaces that broke during testing and had a ΔT of 700° C. (D) and (E) are surfaces that broke during testing and had a ΔT of 900° C.

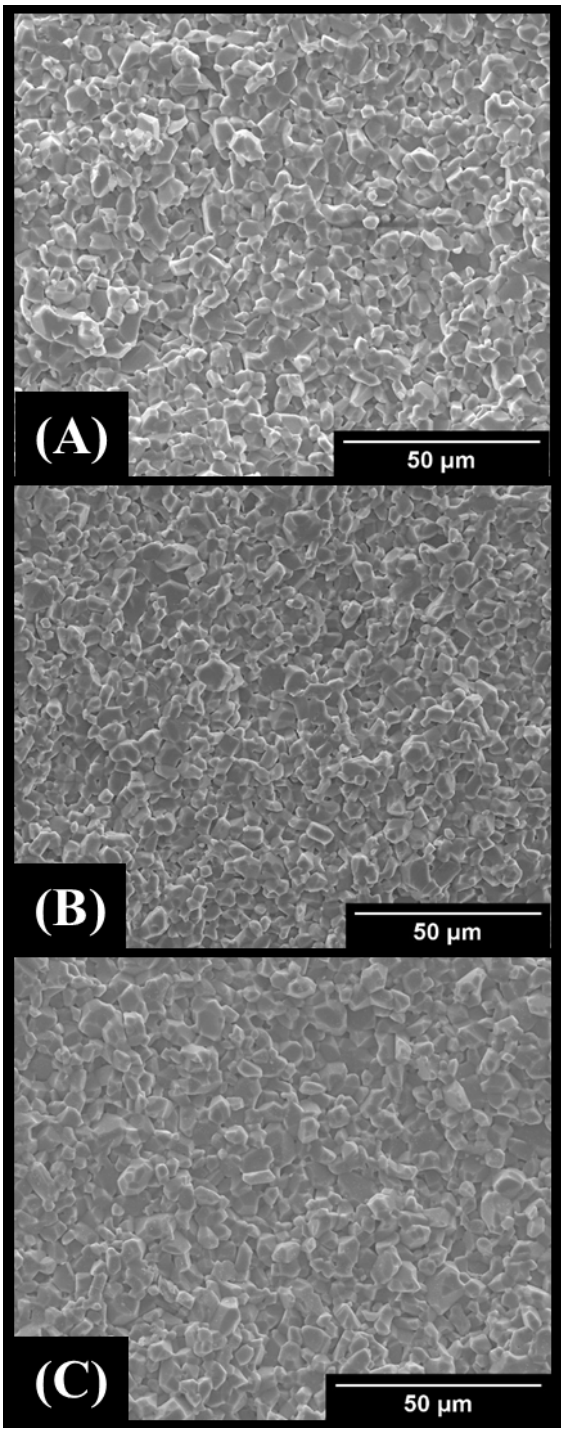

Figure 32. Fracture surface of a printed part that was manually broken and experienced no ΔT. (B) fracture surface that broke during testing and had a ΔT of 700° C. (C) fracture surface that broke during testing and had a ΔT of 900° C.

IV. SUMMARY AND CONCLUSIONS

A desired geometry was successfully produced from alumina (99.8%) via LCM. The geometry originally struggled to survive the debinding process. While it was undergoing the thermal process to remove the organic binder the part would crack. It was seen that the use of a setter plate, produced by the same means as the desired part, resulted the sample not cracking while going through the debinding process. The part was placed on the setter plate for the post processing thermal treatment and resulted in the successful production of the part.

A testing apparatus was designed and produced in order to pressure test the samples. This apparatus allowed the nozzles to be held as they would be in their desired application. The combination of the solenoid valve, controlled via the Arduino, with the tank of industrial grade nitrogen allowed us to quickly and precisely pressurize the samples.

Ink was used to examine the damage that occurred from thermally shocking the samples. Low ΔT samples, 300° C, showed faint lines appearing across the geometry as the cracks are shallow. A higher change in temperature resulted in darker lines, indicating more serve crack propagation. For samples with ΔT of 700° C and 900° C, ink could be seen on the inside of the chamber wall. This shows that critical damage occurred as the cross section of the wall was breached.

Samples that were not thermally shocked could withstand consistent pressure testing of 6.9 MPa (1,000 psi) for over 200 cycles. The samples did not show any signs of damage after being pressurized. In addition, samples that had a ΔT of 300° C could handle 6.9 MPa (1,000 psi) and ΔT of 500° C could handle 3.4 MPa (500 psi), of consistent testing, for over 200 cycles. While the 700° C and 900° C ΔT's could not handle any pressure.

V. FUTURE WORK

Future work includes conducting additional pressure tests to narrow in on exact pressure that these each of the ΔT's could withstand. The ΔT of 500° C samples showed that it could handle a few cycles of being pressurized to 6.9 MPa (1,000 psi) but eventually broke. Samples of ΔT 700° C and 900° C did not have any successful results. Using a lower pressure might yield successful results.

In addition, re-conducting these tests using a different material that would be able to better withstand thermal shock. By not using alumina the samples may be able to withstand the tested pressures at a higher ΔT valve. Silicon nitride (Si_3N_4) shows promise that it could withstand the greater temperature difference than alumina.

Table 2. Calculated Thermal Shock Figure Of Merit For Several Materials Suggested As Possible Material Choices For Future Work [34, 35]

	λ Thermal Conductivity (W/m*K)	σ Strength (MPa)	α Thermal Expansion (1 * 10-6/°C)	E Modulus of Elasticity (GPa)	Thermal Shock Figure of Merit
Al_2O_3	32	380	7.2 - 8.0	380	4.2
ZrO_2	3	710 - 1,470	10.0 - 11.4	200 - 220	1.5
ZTA	24	621	6.0 - 7.1	380	6.0
Si_3N_4	25 - 54	580 - 1,020	2.4 - 3.5	290 - 300	36.3
SiC	60 - 200	450 - 540	3.7 - 4.5	430 - 440	36.1

VI. **REFERENCES**

1. Klocke, F., Modern Approaches for the Production of Ceramic Components. *Journal of the European Ceramic Society* **1997,** *17* (2-3), 457-465.
2. Homa, J.; Schwentenwein, M., A Novel Additive Manufacturing Technology for High-Performance Ceramics. In *Advanced Processing and Manufacturing Technologies for Nanostructured and Multifunctional Materials, Proceedings of the International Conference on Advanced Ceramics and Composites,* Daytona Beach, Florida, January 27-31, 2014; Vol. 35.
3. Pelz, J. S.; Ku, N.; Meyers, M. A.; Vargas-Gonzalez, L. R., Additive Manufacturing of Structural Ceramics: A Historical Perspective. *Journal of Materials Research and Technology* **2021**, *15* (November-December 2021), 670-695.
4. Shulman, H., Additive Manufacturing of High-Performance Ceramics*, Proceedings of the The American Ceramic Society Ceramic Materials Short Courses,* Virtually, October 26-29, 2020.
5. Scheithauer, U.; Schwarzer, E.; Moritz, T.; Michaelis, A., Additive Manufacturing of Ceramic Heat Exchanger: Opportunities and Limits of the Lithography-Based Ceramic Manufacturing (LCM). *Journal of Materials Engineering and Performance* **2018**, *27,* 14-20.
6. Mayerhofer, M.; Lepuschitz, W.; Hoebert, T.; Merdan, M.; Schwentenwein, M.; Strasser, T. I., Knowledge-Driven Manufacturability Analysis for Additive Manufacturing. *IEEE Open Journal of the Industrial Electronics Society* **2021**, *2,* 207-223.
7. Felzmann, R.; Gruber, S.; Mitteramskogler, G.; Tesavibul, P.; Boccaccini, A. R.; Liska, R.; Stampfl, J., Lithography-Based Additive Manufacturing of Cellular Ceramic Structures. *Advanced Engineering Materials* **2012**, *14* (12), 1052-1058.
8. Schwentenwein, M.; Homa, J., Additive Manufacturing of Dense Alumina Ceramics. *International Journal of Applied Ceramic Technology* **2014,** *12* (1), 1-7.
9. Lewis, J. A., Colloidal Processing of Ceramics. *Journal of the American Ceramic Society* **2004**, *83* (10), 2341-2359.
10. Wang, J.-C.; Dommati, H.; Hsieh, S.-J., Review of Additive Manufacturing Methods for High-Preformance Ceramic Materials. *The International Journal of Advanced Manufacturing Technology* **2019**, *103,* 2627-2647.
11. Schwentenwein, M.; Schneider, P.; Homa, J., Lithography-based Ceramic Manufacturing: A Novel Technique for Additive Manufacturing of High-Performance Ceramics. *Advances in Science and Technology* **2014**, *88,* 60-64.
12. Schwentenwein, M.; Homa, J., How Can CIM Benefit from Additive Manufacturing? *Ceramics Applications* **2014**.
13. Homa, J.; Patzer, J.; Reiter, R.; Spitzbart, M. Method for the Layered Construction of a Shaped Body. US 10,864,675 B2, 2016.
14. Mitteramskogler, G.; Gmeiner, R.; Felzmann, R.; Gruber, S.; Hofstetter, C.; Stampfl, J.; Ebert, J.; Wachter, W.; Laubersheimer, J., Light Curing Strategies for Lithography-based Additive Manufacturing of Customized Ceramics. *Additive Manufacturing* **2014,** *1-4* (October 2014), 110-118.

15. Reed, J. S., *Principles of Ceramics Processing*. A Wiley-Interscience Publication: 1995.
16. Schlacher, J.; Lube, T.; Harrer, W.; Mitteramskogler, G.; Schwentenwein, M.; Danzer, R.; Bermejo, R., Strength of Additive Manufactured Alumina. *Journal of the European Ceramic Society* **2020,** *40* (14), 4737-4745.
17. ASTM International. *Standard Test Methods for Determining Average Grain Size*; ASTM E112-12; West Conshohocken, PA, 2012. DOI: 10.1520/E0112-12.
18. Hull, S., Detection of Cracks in Ceramics used in Electronic Devices using Light Scattering. In *Nondestructive Characterization of Materials VI*, Jr., R. E. G.; Kozaczek, K. J.; Ruud, C. O., Eds. 1994; pp 469-477.
19. Maensiri, S.; Roberts, S. G., Thermal Shock of Ground and Polish Alumina and Al_2O_3/SiC Nanocomposites. *Journal of the European Ceramic Society* **2002**, *22* (16), 2945-2956.
20. Hasselman, D. P. H., Thermal Stress Resistance of Engineering Ceramics. *Materials Science and Engineering* **1985,** *71* (May 1985), 251-264.
21. Kingery, W. D., Factors Affecting Thermal Stress Resistance of Ceramic Materials. *Journal of the American Ceramic Society* **1955,** *38* (1), 3-15.
22. Pham, H. V.; Maruoka, D.; Nanko, M., Influences of Al_2O_3 Grain Size on High-Temperature Oxidation of Nano-Ni/Al_2O_3 Composites. *Journal of Asian Ceramic Societies* **2016,** *4* (1), 120-123.
23. Zhao, J.; Ai, X.; Deng, J.; Wang, Z., A Model of the Thermal Shock Resistance Parameter for Functionally Gradient Ceramics. *Materials Science and Engineerign A* **2004,** *382* (1-2), 23-29.
24. Hasselman, D. P. H.; Heller, R. A., *Thermal Stresses in Severe Environments*. Plenum Press: 1980.
25. Hasselman, D. P. H., Figures-of-Merit for the Thermal Stress Resistance of High-Temperature Brittle Materials: a Review. *Ceramurgia International* **1978,** *4* (4), 147-150.
26. Koyama, T.; Nishiyama, A.; Niihara, K., Effect of Grain Morphology and Grain Size on the Mechanical Properties of Al_2O_3 Ceramics. *Journal of Materials Science* **1994,** *29*, 3949-3954.
27. Pelleg, J., *Mechanical Properties of Ceramics*. Springer, Cham: 2014; pp 617-704.
28. Kambale, K. R.; Mahajan, A.; Butee, S. P., Effect of Grain Size on the Properties of Ceramics. *Metal-Powder.net* **2019,** *74* (3), 130-136.
29. Canon, R. F.; Roberts, J. T. A.; Beals, R. J., Defromation of UO_2 at High Temperatures. *Journal of the American Ceramic Society* **1971,** *54* (2), 105-112.
30. Li, K.; Guo, L., Evaluation of Thermal Shock Resistance of Alumina Ceramics. *Scientific.Net* **2011,** *492*, 333-336.
31. Dalgleish, B. J.; Fakhr, A.; Pratt, P. L.; Rawlings, R. D., The Fracture Toughness - Microstructure Relationship of Alumina-Based Ceramics. In *Advances in Fracture Research Vol. 6, Proceedings of the 5th International Conference on Fracture*, Cannes, France, March 29 - Apirl 3, 1981.
32. *Breviary Technical Ceramics 5.4.3 Thermal Shock Resistance*. http://www.keramverband.de/brevier_engl/5/4/5_4_3.htm (accessed 2021-06-07).

33. Sherman, D.; Schlumm, D., Thickness Effect in Thermal Shock of Alumina Ceramics. *Scripta Materialia* **2000,** *42* (8).
34. Kyocera Corporation, Corporate Fine Ceramics Group, *Characteristics of Kyocera Fine Ceramics*. https://global.kyocera.com/prdct/fc/product/pdf/material.pdf (accessed 2021-08-02).
35. Superior Technical Ceramics Corporation, Ceramic Materials Solutions, *Zirconia-Toughened Alumina Specifications.* https://www.ceramics.net/sites/default/files/files/ZTA%20Material%20Property%20Chart%201page.pdf (accessed 2021-08-02).